This article has been accepted for publication in a future issue of this journal, but has not been fully edited. Content may change prior to final publication. Citation information: DOI 10.1109/TCOMM.2021.3097726, IEEE Transactions on Communications

Deep Learning Optimized Sparse Antenna Activation for Reconfigurable Intelligent Surface Assisted Communication

Shunbo Zhang, Shun Zhang, *Senior Member, IEEE*, Feifei Gao, *Fellow, IEEE*, Jianpeng Ma, *Member, IEEE*, Octavia A. Dobre, *Fellow, IEEE*

***Abstract*—Reconfigurable intelligent surface (RIS) is a revolutionary technology for achieving high rate and large coverage in future wireless networks by smartly reflecting the signals with adjustable phase shifts. To design the reflection beamforming, accurate individual channel state information is required at the RIS, which is a challenge task due to the lack of signal processing ability in passive mode. In this paper, we add signal processing units for a few antennas at the RIS to partially acquire the channels and extrapolate them to the full channels, in which the active antenna selection is a key point but has not been addressed yet. We construct an active antenna selection network that utilizes the probabilistic sampling theory to select the optimal locations of these active antennas. With this active antenna selection network, we further design two deep learning-based schemes, i.e., the channel extrapolation scheme and the beam searching scheme. The former utilizes the selection network and a convolutional neural network to extrapolate the full channels from the partial channels, while the latter adopts a fully-connected neural network to achieve the direct mapping from the partial channels to the optimal beamforming vector with maximal transmission rate. Simulation results show that the proposed optimal antenna selection outperforms the trivial uniform antenna selection, and the performance of beam searching is more stable than that of channel extrapolation with fewer active antennas.**

***Index Terms*—Deep learning, active RIS antenna elements, probabilistic sampling theory, channel extrapolation, beam searching**

I. Introduction

An emerging hardware technology called reconfigurable intelligent surface (RIS) can effectively capture the performance gain of the massive radiating elements, which has been considered as a promising technique for both beyond 5G and 6G [1]–[3]. The RIS consists of numerous reconfigurable reflecting elements, each of which is able to shift the phase of the incident electromagnetic waves by electronic controls [4]–[11]. With the equipped elements, RIS can efficiently create a smart, programmable and controllable wireless propagation environment [12]–[16].

Conventional, the reflecting elements of RIS are working in passive mode, which leads to very low energy consumption [17]–[19]. One objective of the most existing RIS works is to design the beamforming [20]–[23]. Guo *et al.* proposed a low-complexity algorithm to jointly design the beamforming and the phase shifting at RIS elements to maximize the weighed sum-rate of all users in [20]. In [21], Ying *et al.* proposed a geometric mean decomposition-based beamforming for RIS-assisted millimeter wave hybrid multi-input multi-output (MIMO) systems. Wu *et al.* jointly optimized the active transmit beamforming and the passive reflecting beamforming to minimize the total transmit power for the RIS-aided systems [22], and extended their work to the discrete phase shift case in [23].

Another object of the existing RIS works is to estimate the channels [24]–[29]. In [24], Jensen *et al.* designed a least square (LS)-based channel estimation scheme for the RIS-aided communication systems. Nadeem *et al.* provided a minimum mean squared error (MMSE)-based channel estimation scheme in RIS-assisted multi-user multiple-input single-output (MISO) systems [25]. In [26], Guan *et al.* deployed two anchor nodes near the RIS to acquire the cascaded channels for all users. However, the above works with fully-passive RIS can only obtain the cascaded channels, while designing the reflecting beamforming needs the individual channels. In passive mode, RIS elements have no digital signal processing function while feeding back the estimated channel state information (CSI) at receiver to the RIS for phase shifting may cost huge overhead [27]. One solution is to place baseband signal processing units at the RIS and then directly estimate the individual channels, namely, some RIS elements could be activated during the communications process. Then, the entire communication process can be divided into two stages, i.e., the channel estimation stage and the data transmission stage. The channel estimation stage would bring extra power cost, but can simplify the signal processing of the data transmission. In [28], Jung *et al.* utilized the RIS with signal processing units to

The work of Shunbo Zhang, Shun Zhang, and Jianpeng Ma was supported in part by the National Key Research and Development Program of China under Grant 2017YFB1010002; in part by the National Natural Science Foundation of China under Grant 61871455, Grant 61931017, and Grant 61901329; and in part by the China Postdoctoral Innovation Talent Support Program under Grant BX20190265. The work of Feifei Gao was supported by the National Natural Science Foundation of China under Grant 61831013. The work of Octavia A. Dobre was supported by the Natural Sciences and Engineering Research Council of Canada (NSERC) through the Discovery Program. *(Corresponding author: Shun Zhang.)*

Shunbo Zhang, Shun Zhang, and Jianpeng Ma are with the State Key Laboratory of Integrated Services Networks, Xidian University, Xi'an 710071, P. R. China (e-mail: sbzhang_19@stu.xidian.edu.cn, zhangshunsdu@xidian.edu.cn, jpmaxdu@gmail.com).

Feifei Gao is with Institute for Artificial Intelligence, Tsinghua University (THUAI), State Key Lab of Intelligent Technologies and Systems, Tsinghua University, Beijing National Research Center for Information Science and Technology (BNRist), Department of Automation,Tsinghua University Beijing, P.R. China (email: feifeigao@ieee.org).

Octavia A. Dobre is with Faculty of Engineering and Applied Science, Memorial University, St. John's NL AIC-5S7, Canada (e-mail: odobre@mun.ca).

This article has been accepted for publication in a future issue of this journal, but has not been fully edited. Content may change prior to final publication. Citation information: DOI 10.1109/TCOMM.2021.3097726, IEEE Transactions on Communications

obtain the individual CSI by uplink pilot training and analyzed the performance of the system with a well-defined uplink frame structure and pilot contamination. Alexandropoulos *et al.* presented an RIS architecture comprising of passive elements, a simple controller, and a single radio frequency (RF) chain for baseband measurements [29]. Besides, they proposed an alternating optimization approach for explicit estimation of channel gains at RIS during dedicated training slots.

All these works [20]–[29] are closely dependent on hypothetical mathematical models. In practical communication scenario, the radio scattering conditions can be very complicated, which makes the hypothetical mathematical model hardly match the actual communication model. Deep learning (DL), a revolutionary technology that aims to obtain certain performance gain via the data-driven manner rather than the specific mathematical models, has undergone a renaissance with excellent performance [30]–[40]. Recently, DL has been adopted to implement the signal processing tasks in RIS systems and has achieved remarkable performance. In [41], Khan *et al.* proposed a DL method for channel estimation and phase angles design in RIS-assisted wireless communication systems. Gao *et al.* developed an unsupervised learning-based approach for passive beamforming in RIS-assisted communication systems [42]. In [43], Huang *et al.* proposed a joint design of transmit beamforming and phase shifts based on deep reinforcement learning technique, which also has a standard formulation and low complexity.

To avoid large power consumption, the number of the activated elements on RIS should be limited. In [44], Alrabeiah *et al.* selected a subset of the antennas to estimate the channels and leveraged the DL tool to extrapolate the channels to all antennas. Taha *et al.* used randomly configured active elements to sub-sample the channels and developed a DL-based solution to optimize the beamforming vector of RIS [45]. Obviously, the performance of the channel extrapolation and the beamforming design is closely related to the selection of the active RIS elements. One commonly adopted way is to use a uniform activation pattern as did in [46]. However, the best activation pattern should be related to the locations of users and the RIS, together with the electromagnetic scattering environment, while the uniform activation pattern may not be the optimal solution.

In this paper, we investigate the active element-aided RIS communication system and aim to maximize the achievable rate for data transmission. We add a few active elements at the RIS and construct an active antenna selection network to find the optimal locations of these elements, where the probabilistic sampling theory is utilized to model the selection of the activated RIS elements as a continuous and differentiable function. Furthermore, we design two schemes, i.e., the channel extrapolation scheme and the beam searching schemes. The former includes the active antenna selection network and a convolutional neural network (CNN)-based channel extrapolation network that aims to extrapolates the full channels from the estimated partial channels, while the latter adopts the active antenna selection network and a fully-connected neural network (FNN)-based beam searching network that directly maps from the estimated partial channels to the optimal beamforming vector. Lastly, we design a proper network off-line training to optimize both the RIS activation pattern and the respective neural network (NN) of the two schemes.

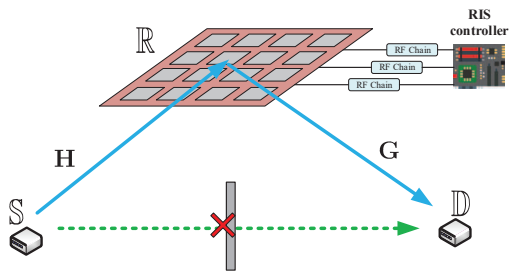

Fig. 1. The RIS-assisted communication system model.

The rest of this paper is organized as follows. Section II presents the system model and the problem formulation. Section III introduces the DL-based channel extrapolation scheme. Section IV describes the DL-based beam searching scheme. Section V provides the numerical results and Section VI draws conclusions.

Notations: Denote lowercase (uppercase) boldface as vector (matrix). $(\cdot)^H$, $(\cdot)^T$, $(\cdot)^*$, and $(\cdot)^\dagger$ represent the Hermitian, transpose, conjugate, and pseudo inverse, respectively. $\mathbb{E}\{\cdot\}$ is the expectation operator. $\odot$ and $\otimes$ represent the Hadamard product operator and Kronecker product operator, respectively. Denote $|\mathcal{A}|$ as the number of elements in set $\mathcal{A}$. $[\mathbf{A}]_{i,j}$ and $[\mathbf{A}]_{\mathcal{Q},:}$ (or $[\mathbf{A}]_{:,\mathcal{Q}}$) represent the (i,j)-th entry of $\mathbf{A}$ and the submatrix of $\mathbf{A}$ which contains the rows (or columns) with the index set $\mathcal{Q}$, respectively. $[\mathbf{B}]_{:,:,i}$ is the i-th slice along the third dimension of a 3D matrix $\mathbf{B}$. $v \sim \mathcal{CN}(0,\sigma^2)$ means that v follows the complex Gaussian distribution with zero-mean and variance σ^2. $\|\mathbf{a}\|$ is the ℓ_2-norm of the vector $\mathbf{a}$. The real and imaginary component of x is expressed as $\Re(x)$ and $\Im(x)$, respectively. Moreover, $\mathrm{diag}(\mathbf{x})$ is a diagonal matrix whose diagonal elements are formed with the elements of $\mathbf{x}$.

II. System Model and Problem Formulation

A. RIS-assisted Communication System Model

As depicted in Fig. 1, we consider an RIS-assisted communications system that consists of a single-antenna transmitter $\mathbb{S}$, a single-antenna receiver $\mathbb{D}$, and an RIS $\mathbb{R}$ with $N_v \times N_h = N$ reflecting elements in the form of a uniform planar array (UPA), where N_v and N_h are the number of elements on the vertical and horizontal dimension, respectively. Denote the set of all reflecting elements at $\mathbb{R}$ as $\mathcal{N}$. In particular, $\mathbb{R}$ can assist the communications from $\mathbb{S}$ to $\mathbb{D}$ by reflecting the incident electromagnetic wave with tunable phase shift.

To combat the practical frequency selective fading, we adopt the orthogonal frequency division multiplexing (OFDM) scheme with K subcarriers. Generally, the direct path between $\mathbb{S}$ and $\mathbb{D}$ tends to be blocked by possible obstacles like buildings and human bodies. Hence, we mainly focus on the RIS-assisted link. Define the ℓ-th tap of the time domain

This article has been accepted for publication in a future issue of this journal, but has not been fully edited. Content may change prior to final publication. Citation information: DOI 10.1109/TCOMM.2021.3097726, IEEE Transactions on Communications

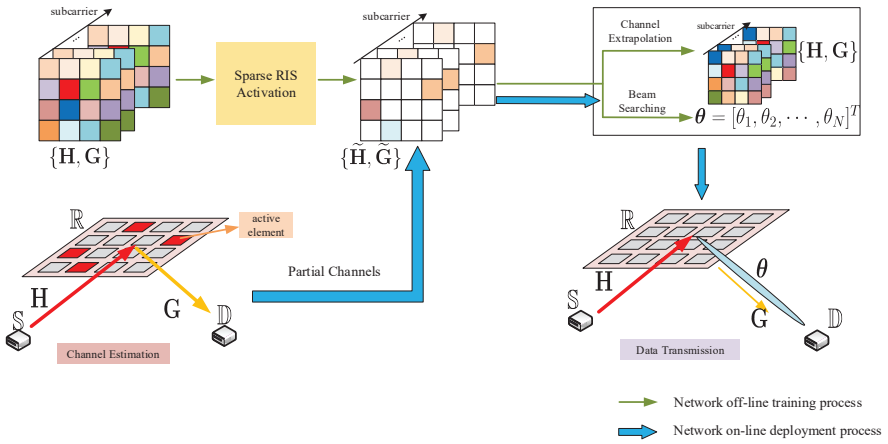

Fig. 2. The architecture of the proposed schemes.

channel from $\mathbb{S}$ to $\mathbb{R}$ as [47]

$$\breve{\mathbf{h}}_\ell = \sum_{p=1}^{P_h} h_{p,f_c}\delta(\ell T_s - \tau_{h,p})\mathbf{a}(\psi_{h,p}, \varphi_{h,p}), \tag{1}$$

where P_h is the number of the scattering paths along the link $\mathbb{S} \to \mathbb{R}$, h_{p,f_c} is the equivalent complex channel gain of the p-th path at carrier frequency f_c, $\tau_{h,p}$ is the time delay, $\delta(\cdot)$ denotes the Dirac function, T_s is the system sampling period, $\mathbf{a}(\psi_{h,p}, \varphi_{h,p}) \in \mathcal{C}^{N\times 1}$ represents the spatial steering vector of $\mathbb{R}$, $\psi_{h,p}$ and $\varphi_{h,p}$ is the angles of arrival (AoAs) at $\mathbb{R}$. The frequency domain channel vector at the k-th subcarrier from $\mathbb{S}$ to $\mathbb{R}$ can be derived as [48]

$$\begin{aligned}\mathbf{h}_k = [\mathbf{H}]_{:,k} &= \frac{1}{\sqrt{K}}\sum_{\ell=0}^{K-1}\breve{\mathbf{h}}_\ell e^{-\jmath 2\pi\frac{\ell k}{K}} \\ &= \frac{1}{\sqrt{K}}\sum_{p=1}^{P_h} h_{p,f_c} e^{-\jmath 2\pi\frac{k\tau_{h,p}}{KT_s}}\mathbf{a}(\psi_{h,p}, \varphi_{h,p}),\end{aligned} \tag{2}$$

where $\mathbf{H} = [\mathbf{h}_0, \mathbf{h}_1, \cdots, \mathbf{h}_{K-1}] \in \mathcal{C}^{N\times K}$ is the frequency domain channel matrix between $\mathbb{S}$ and $\mathbb{R}$. The channel vector $\mathbf{g}_k \in \mathcal{C}^{N\times 1}$ at the k-th subcarrier from $\mathbb{D}$ to $\mathbb{R}$ can be similarly defined as (2), and $\mathbf{g}_k^T$ is the channel from $\mathbb{R}$ to $\mathbb{D}$ by reciprocity. Define $\mathbf{G} = [\mathbf{g}_0, \mathbf{g}_1, \cdots, \mathbf{g}_{K-1}] \in \mathcal{C}^{N\times K}$ as the frequency domain channel matrix between $\mathbb{D}$ and $\mathbb{R}$.

Due to the substantial path loss, we only consider the signal reflection by $\mathbb{R}$ for the first time and ignore those reflected by $\mathbb{R}$ for two or more times. Then, the received signal of the k-th subcarrier at $\mathbb{D}$ can be written as

$$y_k = \mathbf{g}_k^T\boldsymbol{\Theta}\mathbf{h}_k s_k + n_k = (\mathbf{g}_k \odot \mathbf{h}_k)^T\boldsymbol{\phi}s_k + n_k, \tag{3}$$

where s_k is the signal at the k-th subcarrier from $\mathbb{S}$, $\boldsymbol{\Theta} = \text{diag}(\boldsymbol{\phi}) = \text{diag}(e^{\jmath\theta_1}, \cdots, e^{\jmath\theta_N})$ is a diagonal matrix, $\boldsymbol{\phi} = [e^{\jmath\theta_1}, \cdots, e^{\jmath\theta_N}]^T$ denotes the reflection beamforming vector of $\mathbb{R}$, and $n_k \sim \mathcal{CN}(0, \sigma^2)$ is the additive white Gaussian noise (AWGN) at $\mathbb{D}$. Moreover, define $\boldsymbol{\theta} = [\theta_1, \theta_2, \cdots, \theta_N]^T$ as the phase shifts of all the elements on $\mathbb{R}$ and denote $\frac{\mathbb{E}[|s_k|^2]}{\sigma^2} = \frac{P_t}{K\sigma^2}$ as the signal-to-noise ratio (SNR), where P_t is the transmit power.

In this paper, $\mathbb{R}$ can be reconfigured by a controller connected with RF chains, and the corresponding phase shift is set as a finite number of discrete values that belong to the quantized set $\mathcal{A} \triangleq \{0, \Delta, \cdots, (2^b-1)\Delta\}$, where b is the number of quantization bits and $\Delta = 2\pi/2^b$ represents the quantization step size. Since $\mathbb{R}$ has N digital phase shift elements, the reflection beamforming vector $\boldsymbol{\phi}$ would have 2^{bN} different choices.

B. Problem Formulation

The effective data are conveyed along the link $\mathbb{S} \to \mathbb{R} \to \mathbb{D}$ with center frequency f_c. The aim is to maximize the achievable rate at $\mathbb{D}$ over all possible $\boldsymbol{\phi}$'s, i.e.,

$$(\text{P1}): \max_{\boldsymbol{\phi}^\star} \; R = \frac{1}{K}\sum_{k=0}^{K-1}\log_2\left(1 + \left|(\mathbf{g}_k \odot \mathbf{h}_k)^T\boldsymbol{\phi}s_k\right|^2/\sigma^2\right) \tag{4}$$

$$\text{s.t.} \;\; \theta_n \in \mathcal{A} = \{0, \Delta, \cdots, (2^b-1)\Delta\}, \forall n \in \mathcal{N} \tag{5}$$

$$|\phi_n| = 1, \forall n \in \mathcal{N}. \tag{6}$$

It can be checked that to find the optimal beamforming vector $\boldsymbol{\phi}^\star$, full channels $\mathbf{H}$ and $\mathbf{G}$ need to be acquired at $\mathbb{R}$, which is a hard task for the traditional RIS due to the lack of signal processing function. Intuitively, we can set a small part of the RIS elements, i.e., a set $\mathcal{M}$, as active sensors to obtain the partial channels between the transceivers and the RIS. Then it is possible to extrapolate the full channels from these partial ones, where $|\mathcal{M}| = M \ll N$ [44]. Hence, how to design an efficient channel extrapolation scheme is the first challenge that needs to be solved. Due to the limited number of RF chains and the requirement of low power cost, the number of active elements should be as small as possible, which may limit the performance of the channel extrapolation. Thus, how to approach the maximal achievable rate in (4) by finding a quasi-optimal beamforming vector with fewer active elements is the second challenge that needs to be solved. Note that the selection of the active antennas, i.e., the activation pattern $\mathcal{M}$, is crucial to overcome the above two challenges, however, this problem has not been solved to the best of the authors' knowledge. Next, we design two different DL-based schemes, named channel extrapolation scheme and

This article has been accepted for publication in a future issue of this journal, but has not been fully edited. Content may change prior to final publication. Citation information: DOI 10.1109/TCOMM.2021.3097726, IEEE Transactions on Communications

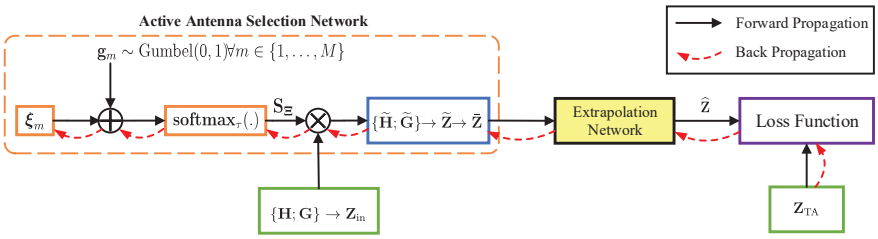

Fig. 3. The structure of the designed DL-based channel extrapolation scheme.

beam searching scheme, to separately address the two aforementioned challenges. In both schemes, the activation pattern is optimized through the probabilistic sampling theory. For both schemes, the corresponding off-line training and on-line deployment are introduced. The unified architecture of these two schemes is shown in Fig. 2.

III. Deep Learning-based Channel Extrapolation Scheme

As presented in Section II, a main challenge for the RIS-assisted communication system is the acquirement of the full channels $\mathbf{H}$ and $\mathbf{G}$ when designing the optimal beamforming vector $\phi^\star$. Traditionally, the receiver $\mathbb{D}$ can perform channel estimation to obtain the cascaded channel of $\mathbf{H}$ and $\mathbf{G}$ and feed it back to $\mathbb{R}$. However, the overheads of the channel estimation and the feedback would be high due to the massive number of reflecting elements on $\mathbb{R}$. To overcome this bottleneck, we add signal processing functions to a small part $\mathcal{M}$ of the RIS reflecting elements $\mathcal{N}$ and utilize these active antennas to acquire the individual channels between the transceivers and the RIS. Define the channels between the active antennas $\mathcal{M}$ and the transceivers as two $M \times K$ matrices $\widetilde{\mathbf{H}} = [\mathbf{H}]_{\mathcal{M},:}$ and $\widetilde{\mathbf{G}} = [\mathbf{G}]_{\mathcal{M},:}$. Since DL can effectively extract the latent and complex relationship among various datasets such as different channels, we design a DL-based channel extrapolation scheme to optimize both the activation pattern and the channel extrapolation ability. The overall flow of the designed scheme is expressed as

$$\{\mathbf{H},\mathbf{G}\} \xrightarrow{\text{spatial sub-sampling}} \{\widetilde{\mathbf{H}},\widetilde{\mathbf{G}}\} \xrightarrow{\text{channel extrapolation}} \{\widehat{\mathbf{H}},\widehat{\mathbf{G}}\}, \tag{7}$$

where $\widehat{\mathbf{H}} \in \mathcal{C}^{N\times K}$ and $\widehat{\mathbf{G}} \in \mathcal{C}^{N\times K}$ denote the recovery of $\mathbf{H}$ and $\mathbf{G}$, respectively. The structure of (7) is shown in Fig. 3, which contains the active antenna selection network and the channel extrapolation network.

A. Active Antenna Selection Network

Define the spatial compression ratio as $r = \frac{M}{N}$. The effect of the active antenna selection network can be expressed as a sub-sampling matrix $\mathbf{S}$ on the full channel $\mathbf{H}$ and $\mathbf{G}$ as

$$\widetilde{\mathbf{H}} = \mathbf{S}\mathbf{H}, \tag{8}$$

$$\widetilde{\mathbf{G}} = \mathbf{S}\mathbf{G}, \tag{9}$$

where $\mathbf{S} = [\mathbf{s}_0^T, \mathbf{s}_1^T, \ldots, \mathbf{s}_{M-1}^T]^T \in \{0,1\}^{M\times N}$ is a binary matrix, and its m-th row vector $\mathbf{s}_m$ contains only one non-zero entry.

Generally, the back propagation (BP) algorithm is involved when training the DL model. However, since the utilization of $\mathbf{S}$ is a discrete combination operation, it is difficult to define the gradient differentiation. To overcome this obstacle, we define a trainable matrix $\mathbf{\Xi} = [\boldsymbol{\xi}_0^T, \boldsymbol{\xi}_1^T, \cdots, \boldsymbol{\xi}_{M-1}^T]^T \in \mathcal{R}^{M\times N}$, whose m-th row vector is an independent categorical distribution $\boldsymbol{\xi}_m$ and the n-th entry of $\boldsymbol{\xi}_m$ is an unnormalized log-probability (logit) $\xi_{m,n}$. Then, we leverage the probabilistic sampling strategy and replace $\mathbf{S}$ with a learned sub-sampling matrix $\mathbf{S}_{\mathbf{\Xi}}$, whose elements are controlled by $\mathbf{\Xi}$.

Since the DL model can only deal with real-valued numbers, we first separate the real and imaginary parts of $\mathbf{H}$ and $\mathbf{G}$, and then collect them into an $N \times K \times 4$ real-valued 3D matrix $\mathbf{Z}_{\text{in}} = [\Re(\mathbf{H}); \Im(\mathbf{H}); \Re(\mathbf{G}); \Im(\mathbf{G})]$ as the input of the active antenna selection network. The selection network implements the selection operation on $\mathbf{H}$ and $\mathbf{G}$ to obtain $\widetilde{\mathbf{H}}$ and $\widetilde{\mathbf{G}}$ by sub-sampling $\mathbf{Z}_{\text{in}}$ along its first dimension as

$$\widetilde{\mathbf{Z}} = [\Re(\widetilde{\mathbf{H}}); \Im(\widetilde{\mathbf{H}}); \Re(\widetilde{\mathbf{G}}); \Im(\widetilde{\mathbf{G}})] = F_{\mathbf{\Xi}}(\mathbf{Z}_{\text{in}}), \tag{10}$$

where $\widetilde{\mathbf{Z}} \in \mathcal{R}^{M\times K\times 4}$ denotes the original output of the selection network, while $F_{\mathbf{\Xi}}(\cdot)$ represents the sub-sampling function and is expressed as

$$[\widetilde{\mathbf{Z}}]_{:,:,i} = \mathbf{S}_{\mathbf{\Xi}}[\mathbf{Z}_{\text{in}}]_{:,:,i}, i = 0,1,2,3. \tag{11}$$

Remark 1: The considered system can be extended to the multiple-antenna transmitter scenario. Assume the transmitter $\mathbb{S}$ is equipped with N_t antennas in the form of a uniform linear array. The frequency domain channel between $\mathbb{S}$ and $\mathbb{R}$ is expanded to a 3D matrix $\mathbf{H} \in \mathcal{C}^{N\times N_t\times K}$. The input of the active antenna selection network is enlarged to $\mathbf{Z}_{\text{in}}^{\text{new}} = [\Re([\mathbf{H}]_{:,0,:}); \Im([\mathbf{H}]_{:,0,:}); \cdots; \Re([\mathbf{H}]_{:,N_t-1,:}); \Im([\mathbf{H}]_{:,N_t-1,:}); \Re(\mathbf{G}); \Im(\mathbf{G})] \in \mathcal{C}^{N\times K\times(2N_t+2)}$. Compared with the single-antenna transmitter scenario, the size of the input of NNs would be enlarged under the multiple-antenna transmitter scenario; however, the fundamental structures of the designed NNs still maintain. To better present our core idea, we only consider the single-antenna transmitter scenario in this paper.

Within the probabilistic sampling theory, $\mathbf{s}_m$ can be defined as [49]

$$\mathbf{s}_m = \text{one\_hot}(c_m), \tag{12}$$

where $\text{one\_hot}(\cdot)$ denotes the one-hot encoding operation, and $c_m \sim \text{Cat}(N, \boldsymbol{\pi}_m)$ is a categorical random variable with $\boldsymbol{\pi}_m = [\pi_{m,0}, \pi_{m,1}, \cdots, \pi_{m,N-1}]$ containing N class probabilities. For different categorical variables, i.e., $\forall m_1 \neq m_2$, c_{m_1} and c_{m_2} are independent with each other. Note that the result

This article has been accepted for publication in a future issue of this journal, but has not been fully edited. Content may change prior to final publication. Citation information: DOI 10.1109/TCOMM.2021.3097726, IEEE Transactions on Communications

of $\text{one\_hot}(c_m)$ is a $1 \times N$ unit-vector and the index of the non-zero entry corresponds to the class of the drawn sample. The larger $\pi_{m,n}$ means that the m-th rows of $\widetilde{\mathbf{H}}$ and $\widetilde{\mathbf{G}}$ can be separately achieved from the n-th rows of $\mathbf{H}$ and $\mathbf{G}$ with higher probability, namely, the n-th RIS element in $\mathcal{N}$ will be activated with higher priority. Furthermore, we reparameterize $\pi_{m,n}$ with $\xi_{m,n}$ by using a softmax function as

$$\pi_{m,n} = \frac{\exp(\xi_{m,n})}{\sum_{n'=0}^{N-1} \exp(\xi_{m,n'})}. \tag{13}$$

In order to obtain an effective sample from the categorical distribution, we resort to the Gumbel-Max trick and generate a realization of c_m as [50]

$$c'_m = \arg\max_n \{\xi_{m,n} + w_{m,n}\}, \tag{14}$$

where $\{w_{m,0}, w_{m,1}, \cdots, w_{m,N-1}\}$ are independent and identically distributed samples following the $\text{Gumbel}(0,1)$ distribution. Correspondingly, $\mathbf{s}_m$ can be achieved from c'_m as

$$\mathbf{s}_m = \text{one\_hot}\{\arg\max_n \{\xi_{m,n} + w_{m,n}\}\}. \tag{15}$$

Remark 2: The purpose of using the Gumbel distribution is to exactly sample from the distribution that we are learning, which fully exploits the property that adding Gumbel noise does not change the original distribution. We show the detailed proof in Appendix A.

However, when conducting the above operation from $m = 0$ to $M-1$, the same row in $\mathbf{H}$ and $\mathbf{G}$, i.e., the same RIS antenna element, may be repeatedly selected many times. To avoid this situation, we dynamically exclude the categories that have already been chosen. Then, we renormalize the logits of the remaining categories and further implement the Gumbel-Max trick.

When training the selection network, $\boldsymbol{\xi}_m$ is iteratively updated through the BP to complete the active antenna selection. However, since the operator $\arg\max$ is non-differentiable, we resort to the softmax_τ function as a continuous and differentiable approximation of $\text{one\_hot}\{\arg\max\}$, where $\text{softmax}_\tau(\mathbf{x}) = \frac{\exp\{\mathbf{x}/\tau\}}{\sum_{i=0}^{N-1}\exp\{x_i/\tau\}}$ and the temperature τ controls the softness of softmax_τ. Then, there is [49]

$$\begin{aligned}\mathbf{s}_m &= \lim_{\tau\to 0} \text{softmax}_\tau(\boldsymbol{\xi}_m + \mathbf{w}_m) \\ &= \lim_{\tau\to 0} \frac{\exp\{(\boldsymbol{\xi}_m + \mathbf{w}_m)/\tau\}}{\sum_{n=0}^{N-1}\exp\{(\xi_{m,n} + w_{m,n})/\tau\}},\end{aligned} \tag{16}$$

where $\mathbf{w}_m = [w_{m,0}, w_{m,1}, \cdots, w_{m,N-1}]$ is the $1\times N$ Gumbel noise vector. Note that lower τ means the generated Gumbel-Softmax distribution $\text{softmax}_\tau(\boldsymbol{\xi}_m + \mathbf{w}_m)$ is closer to the categorical distribution. During the selection network training, τ is gradually reduced to approach the true discrete distribution. The first-order partial derivative of $\mathbf{s}_m$ with respect to $\boldsymbol{\xi}_m$ can be written as

$$\frac{\partial \mathbf{s}_m}{\partial \boldsymbol{\xi}_m^T} = \frac{\partial}{\partial \boldsymbol{\xi}_m^T}\mathbb{E}_{\mathbf{w}_m}\left[\text{softmax}_\tau(\boldsymbol{\xi}_m + \mathbf{w}_m)\right],\ \tau > 0. \tag{17}$$

In order to achieve a faster co-adaptation of the channel extrapolation network with different RIS activation patterns during training, we fill zeros into $\widetilde{\mathbf{Z}}$ after the sub-sampling operation and feed the data related with all RIS antenna elements into the following channel extrapolation network rather than those at the M activated antennas. Then, we have

$$\bar{\mathbf{Z}} = ZF(\widetilde{\mathbf{Z}}), \tag{18}$$

where $\bar{\mathbf{Z}} \in \mathcal{R}^{N\times K\times 4}$ represents the processed output of the selection network and the function $ZF(\cdot)$ is the zero-filling operation. Note that the elements of the non-zero rows in $\bar{\mathbf{Z}}$ are consistent with the elements in $\widetilde{\mathbf{Z}}$, and the locations of these elements in $\bar{\mathbf{Z}}$ are the same as their initial ones in $\mathbf{Z}_{\text{in}}$.

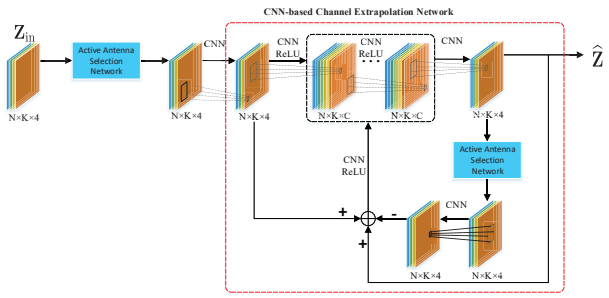

Fig. 4. The structure of the proposed channel extrapolation network.

TABLE I
THE STRUCTURE OF THE CNN-BASED CHANNEL EXTRAPOLATION NETWORK.

Name	Parameter
Number of proximal-gradient iterations	N_p
Number of convolutional layers in each iteration	N_q+2
Total number of convolutional layers	N_c=1+$N_p\times(N_q+2)$
Size of convolutional kernel in the l-th layer	$H\times W\times D_l$
Number of zero-padding	P
Convolutional stride	S

B. Channel Extrapolation Network

The channel extrapolation network aims to simultaneously extrapolate the full channels $\mathbf{H}$ and $\mathbf{G}$ from the sub-sampled channels $\widetilde{\mathbf{H}}$ and $\widetilde{\mathbf{G}}$. Since the channel matrices $\widetilde{\mathbf{H}}$, $\widetilde{\mathbf{G}}$, $\mathbf{H}$ and $\mathbf{G}$ are all 2D matrices, it is reasonable to utilize CNN to conduct the extrapolation task. To obtain an efficient extrapolation performance, we resort to the iterative proximal-gradient algorithm [49], which is dedicated to solving the ill-posed linear measurement problem in (8) and (9). The structure of the CNN-based channel extrapolation network is shown in Fig. 4. The output of the channel extrapolation network is expressed as

$$\widehat{\mathbf{Z}} = [\Re(\widehat{\mathbf{H}}); \Im(\widehat{\mathbf{H}}); \Re(\widehat{\mathbf{G}}); \Im(\widehat{\mathbf{G}})] = G_{\mathcal{W}_C}(\bar{\mathbf{Z}}), \tag{19}$$

where $\widehat{\mathbf{Z}} \in \mathcal{R}^{N\times K\times 4}$ and the function $G_{\mathcal{W}_C}(\cdot)$ denotes the extrapolation operation learned by CNN, whose trainable parameters set is $\mathcal{W}_C$.

To introduce the channel extrapolation network in a concise way, we list the network structure in TABLE I. Note that in the l-th convolutional layer, the size of the convolutional

kernels is $H \times W \times D_l$, where H, W and D_l represent the height, the width and the depth of the convolutional kernels, respectively. The network parameters, i.e., H, W, P and S, should be designed carefully to ensure that the dimension of each slice remains unchanged after convolution. More details about this part are discussed in Section V and the feasibility of the channel extrapolation is presented in Appendix B.

After obtaining $\widehat{\mathbf{Z}}$, we further combine its real and imaginary parts to obtain the extrapolated full channels $\widehat{\mathbf{H}}$ and $\widehat{\mathbf{G}}$.

C. Off-line Training for Active Antenna Selection and Channel Extrapolation Networks

During the off-line training for both the active antenna selection and channel extrapolation networks, we adopt a dedicated computing device that wired to the RIS controller to train the networks. We first set $\mathbb{R}$ as the fully-active model and use the pilot sequences sent by $\mathbb{S}$ and $\mathbb{D}$ to collect the channels at $\mathbb{R}$'s elements. The RIS controller can collect the CSI from $\mathbb{R}$ and transmit them to the computing device via a wired connection. With these collected data, we can construct the labeled samples for the off-line training of the networks. Then, the computing device can train the active antenna selection and channel extrapolation network to obtain the optimal active antenna pattern and the channel extrapolation ability.

Define $\boldsymbol{\omega}_l$ as the vector containing trainable parameters of the l-th convolutional layer and $\mathcal{W}_C = \{\boldsymbol{\omega}_1, \boldsymbol{\omega}_2, \ldots, \boldsymbol{\omega}_{N_C}\}$ as the parameter set of the channel extrapolation network. The set for off-line training is denoted as $\mathcal{D}$, where $|\mathcal{D}| = N_{tr}$ is the number of off-line training samples. A sample in $\mathcal{D}$ is an input-target pair written as $(\mathbf{Z}_{\text{in}}, \mathbf{Z}_{\text{TA}})$, where $\mathbf{Z}_{\text{TA}}$ is the extrapolation target and is equal to $\mathbf{Z}_{\text{in}}$ since we need to acquire the original full channels. During the off-line training phase, the tunable parameters in $\mathcal{W}_C$ and $\boldsymbol{\Xi}$ are trained by minimizing the mean square error (MSE) between the output $\widehat{\mathbf{Z}}$ and the target $\mathbf{Z}_{\text{TA}}$. Thus, the loss function of the channel extrapolation network is written as

$$\mathcal{L}_c = \frac{1}{4NKM_{tr}} \sum_{\mu=0}^{M_{tr}-1} \sum_{i=0}^{3} \left\| [\mathbf{Z}_{\text{TA}}^{\mu}]_{:,:,i} - [\widehat{\mathbf{Z}}^{\mu}]_{:,:,i} \right\|_F^2, \quad (20)$$

where $\|\mathbf{A}\|_F$ is the Frobenius norm of matrix $\mathbf{A}$ and M_{tr} is the batch size for off-line training.

Besides, we promote the training of the parameters in $\boldsymbol{\Xi}$ towards one-hot distributions through penalizing the high entropy distribution for the active antenna selection network as

$$\mathcal{L}_s = -\sum_{m=1}^{M} \sum_{n=1}^{N} \pi_{m,n} \log \pi_{m,n}. \quad (21)$$

When the parameters for the active antenna selection network and the channel extrapolation network are updated jointly, the resultant optimization of the channel extrapolation scheme is

$$\left\{\widehat{\mathcal{W}}_C, \widehat{\boldsymbol{\Xi}}\right\} = \arg \min_{\mathcal{W}_C, \boldsymbol{\Xi}} (\mathcal{L}_c + \rho \mathcal{L}_s), \quad (22)$$

where the penalty multiplier ρ evaluates the importance of different penalties and $\mathcal{L}_C \triangleq \mathcal{L}_c + \rho \mathcal{L}_s$ is the training loss of the channel extrapolation scheme.

During the off-line training phase, the adaptive moment estimation (Adam) [51] optimizer algorithm is adopted to achieve the optimal model parameters $\widehat{\mathcal{W}}_C$ and $\widehat{\boldsymbol{\Xi}}$. We use the learning rates η_ω and η_ξ to respectively update the parameters in $\mathcal{W}_C$ and $\boldsymbol{\Xi}$ with $\eta_\omega < \eta_\xi$. Moreover, we initially set τ as 5.0 and gradually reduce it to 0.5 during training to approach the discrete distribution. All elements in $\boldsymbol{\Xi}$ are initialized as $\xi_{m,n} \sim \mathcal{N}(0, 0.05)$.

After completing the off-line training, the optimal activation pattern $\mathcal{M}$ can be obtained by extracting $\mathbf{S}_{\widehat{\boldsymbol{\Xi}}}$ from the trained active antenna selection network. Note that $\mathbf{S}_{\widehat{\boldsymbol{\Xi}}}$ is controlled by the parameters in $\widehat{\boldsymbol{\Xi}}$, and the index of the non-zero entry in each row of $\mathbf{S}_{\widehat{\boldsymbol{\Xi}}}$ corresponds to the optimal location of an active antenna element on $\mathbb{R}$. Moreover, the trained channel extrapolation network with parameters $\widehat{\mathcal{W}}_C$ can gain the ability to extrapolate the full channels from the given partial channels. Then, we adjust $\mathbb{R}$ from the fully-active model to the semi-active one, where only a small fraction of the reflection elements are active.

Remark 3: With respect to the trained network, its feasible time depends on the specific RIS deployment scenario. For example, if the RIS is deployed in an indoor scenario where the channel conditions would not change sharply, the trained channel extrapolation network can last for a relative long time. However, in the outdoor scenario, the feasible time of the trained channel extrapolation network will be reduced accordingly due to the rapid change of the channel conditions.

D. On-line Deployment for Channel Extrapolation Network

In the on-line deployment phase, the entire communication process is divided into the channel estimation stage and the data transmission stage. During the channel estimation stage, both the transmitter $\mathbb{S}$ and the receiver $\mathbb{D}$ can simultaneously transmit two orthogonal training blocks of short time duration L_t to the RIS $\mathbb{R}$. Over the frequency domain, the training from $\mathbb{S}$ and $\mathbb{D}$ can be separately written as the $K \times L_t$ matrices $\mathbf{T}_1$ and $\mathbf{T}_2$, where $L_t \geq 2$. The received training signal of the k-th subcarrier at $\mathbb{R}$ is

$$\mathbf{Y}_k = [\widetilde{\mathbf{H}}]_{:,k}[\mathbf{T}_1]_{k,:} + [\widetilde{\mathbf{G}}]_{:,k}[\mathbf{T}_2]_{k,:} + \mathbf{N}_k = \mathbf{A}_k \mathbf{P}_k + \mathbf{N}_k, \quad (23)$$

where $\mathbf{A}_k = \left[[\widetilde{\mathbf{H}}]_{:,k}, [\widetilde{\mathbf{G}}]_{:,k}\right] \in \mathcal{C}^{M \times 2}$, $\mathbf{P}_k = \left[[\mathbf{T}_1]_{k,:}^T, [\mathbf{T}_2]_{k,:}^T\right]^T \in \mathcal{C}^{2 \times L_t}$, and $\mathbf{N}_k \in \mathcal{C}^{M \times L_t}$ is the AWGN matrix with each element distributed according to $\mathcal{CN}(0, \sigma^2)$. By adopting the LS estimator, we can obtain the estimates of $[\widetilde{\mathbf{H}}]_{:,k}$ and $[\widetilde{\mathbf{G}}]_{:,k}$ for the k-th subcarrier, i.e.,

$$\mathbf{A}_{k,LS} = \mathbf{Y}_k \mathbf{P}_k^{\dagger}, \quad (24)$$

where $\mathbf{P}_k^{\dagger} = \mathbf{P}_k^H (\mathbf{P}_k \mathbf{P}_k^H)^{-1}$. We can adopt the LS estimation for all K subcarriers to obtain $\widetilde{\mathbf{H}}$ and $\widetilde{\mathbf{G}}$. Since the designed channel extrapolation scheme mainly focuses on the extrapolation from the partial channels to the full ones, we assume that the SNR is large enough during the channel estimation stage and the partial channels $\widetilde{\mathbf{H}}$ and $\widetilde{\mathbf{G}}$ can be obtained perfectly.

Subsequently, the trained channel extrapolation network can rapidly output the extrapolated channels $\widehat{\mathbf{H}}$ and $\widehat{\mathbf{G}}$ with fed $\widetilde{\mathbf{H}}$

Algorithm 1 The training and deployment for channel extrapolation scheme.

PHASE I: Off-line training phase
Require: Training dataset $\mathcal{D}$, the number of iterations N_{iter}, $\tau_{start} = 5, \tau_{end} = 0.5$, and the initialized trainable parameters $\mathcal{W}_C$ and $\mathbf{\Xi}$.
Compute $\Delta\tau = \frac{\tau_{start}-\tau_{end}}{N_{iter}-1}$
for $i = 1$ to N_{iter} **do**
  Draw mini-batches $\mathcal{D}_m$: a random subset of $\mathcal{D}$
  Draw Gumbel noise vectors $\mathbf{w}_m$ for $m \in \{0, ..., M-1\}$
  Compute $\mathbf{S}_{\mathbf{\Xi}} = [\mathbf{s}_0^T, \mathbf{s}_1^T, \ldots, \mathbf{s}_{M-1}^T]^T$ using $\mathbf{s}_m = \text{one\_hot}\{\arg\max_n\{\xi_{m,n} + w_{m,n}\}\}$ for $m \in \{0, ..., M-1\}$, and dynamically exclude the repeatedly selected elements
  Sub-sample the input as $[\widetilde{\mathbf{Z}}]_{:,:,:,i} = \mathbf{S}_{\mathbf{\Xi}}[\mathbf{Z}_{\text{in}}]_{:,:,:,i}$ for $i = 0, 1, 2, 3$
  Achieve the input of CNN-based channel extrapolation network as $\bar{\mathbf{Z}} = ZF(\widetilde{\mathbf{Z}})$
  Compute the output of CNN-based channel extrapolation network as $\widehat{\mathbf{Z}} = G_{\mathcal{W}_C}(\bar{\mathbf{Z}})$
  Compute the loss function as $\mathcal{L}_C = \mathcal{L}_c + \rho\mathcal{L}_s$
  Set $\tau = \tau_{start} - (i-1)\Delta\tau$
  Update $\frac{\partial}{\partial \boldsymbol{\xi}_m^T}\mathbb{E}_{\mathbf{w}_m}\left[\text{softmax}_\tau(\boldsymbol{\xi}_m + \mathbf{w}_m)\right],\ \tau > 0$
  Use the Adam optimizer to update $\mathcal{W}_C$ and $\mathbf{\Xi}$
end for
Acquire the learned logit matrix $\widehat{\mathbf{\Xi}}$, the optimal activation pattern $\mathcal{M}$ and channel extrapolation network parameters $\widehat{\mathcal{W}}_C$
Determine the locations of the M active antenna elements on $\mathbb{R}$ with $\mathcal{M}$
PHASE II: On-line deployment phase
$\mathbb{R}$ utilizes the M active antenna elements as channel sensors to obtain $\widetilde{\mathbf{H}}$ and $\widetilde{\mathbf{G}}$
Feed $\widetilde{\mathbf{H}}$ and $\widetilde{\mathbf{G}}$ into the trained channel extrapolation network to obtain $\widehat{\mathbf{H}}$ and $\widehat{\mathbf{G}}$
Solve the projection problem in (30) to periodically obtain the phase shift vector $\boldsymbol{\theta}^o$ on $\mathbb{R}$
Adopt $\boldsymbol{\theta}^o$ to implement the communication along the link $\mathbb{S} \to \mathbb{R} \to \mathbb{D}$

and $\widetilde{\mathbf{G}}$. As described in (P1), the next step in the on-line phase is to calculate the optimal reflection beamforming vector $\boldsymbol{\phi}^\star$ with the recovered $\widehat{\mathbf{H}}$ and $\widehat{\mathbf{G}}$. With the monotonicity of the logarithmic function and the independence of noise, (P1) can be equivalently transformed as

$$(\text{P2}):\ \boldsymbol{\phi}^\star = \arg\max_{\boldsymbol{\phi}} \sum_{k=0}^{K-1} \left(\left| \left([\widehat{\mathbf{G}}]_{:,k} \odot [\widehat{\mathbf{H}}]_{:,k} \right)^T \boldsymbol{\phi} \right|^2 \right) \quad (25)$$

$$\text{s.t.}\ \ \theta_n \in \mathcal{A} = \left\{0, \Delta, \cdots, (2^b - 1)\Delta\right\}, \forall n \in \mathcal{N} \quad (26)$$

$$|\phi_n| = 1, \forall n \in \mathcal{N}. \quad (27)$$

Note that without the constraints, the optimal solution can be readily obtained as

$$\boldsymbol{\phi}^\star = \sum_{k=0}^{K-1} \left([\widehat{\mathbf{G}}]_{:,k} \odot [\widehat{\mathbf{H}}]_{:,k} \right)^*. \quad (28)$$

Due to the normalization constraint in (27), we normalize each element in $\boldsymbol{\phi}^\star$ and further obtain

$$\phi_n^\diamond = e^{\jmath\theta_n^\diamond} = \frac{\sum_{k=0}^{K-1} \left([\widehat{\mathbf{G}}]_{:,k}(n) [\widehat{\mathbf{H}}]_{:,k}(n) \right)^*}{\left\| \sum_{k=0}^{K-1} \left([\widehat{\mathbf{G}}]_{:,k}(n) [\widehat{\mathbf{H}}]_{:,k}(n) \right)^* \right\|}, \forall n \in \mathcal{N}, \quad (29)$$

where $[\widehat{\mathbf{G}}]_{:,k}(n)$ and $[\widehat{\mathbf{H}}]_{:,k}(n)$ are separately the n-th element of $[\widehat{\mathbf{G}}]_{:,k}$ and $[\widehat{\mathbf{H}}]_{:,k}$.

Let $\boldsymbol{\phi}^\diamond = [\phi_1^\diamond, \phi_2^\diamond, \cdots, \phi_N^\diamond]^T$ and $\boldsymbol{\theta}^\diamond = [\theta_1^\diamond, \theta_2^\diamond, \cdots, \theta_N^\diamond]^T$. Then, with a pre-defined set of the phase shift range $\mathcal{A}$ for $\boldsymbol{\theta}$, we can achieve the solution $\boldsymbol{\theta}^o$ by solving the following projection problem

$$\boldsymbol{\theta}^o = \arg\min_{\theta_n \in \mathcal{A}} ||\boldsymbol{\theta}^\diamond - \boldsymbol{\theta}||^2. \quad (30)$$

Note that the obtained phase shift vector $\boldsymbol{\theta}^o$ corresponds to the reflection beamforming vector $\boldsymbol{\phi}^o = [e^{\jmath\theta_1^o}, e^{\jmath\theta_2^o}, \cdots, e^{\jmath\theta_N^o}]^T$. Within the subsequent data transmission stage, $\mathbb{R}$ utilizes $\boldsymbol{\theta}^o$ to assist the communication between $\mathbb{S}$ and $\mathbb{D}$. For clarity, we present the details about the off-line training and the on-line deployment of the channel extrapolation scheme in Algorithm 1.

IV. Deep Learning-based Beam Searching Scheme

Due to the requirement of low power cost for the RIS, we need to further reduce the number of active antenna elements compared with the channel extrapolation scheme and approach the maximal achievable rate for data transmission. We first adopt a pre-define codebook $\mathcal{B}$ which contains the candidate reflection beamforming vector $\boldsymbol{\phi}$ and is in the same order of N. The more detailed design of the codebook $\mathcal{B}$ is presented in Section V. It is worth noting that the codebook $\mathcal{B}$ is a suboptimal option compared with the quantized set $\mathcal{A}$ but can reduce the training overhead. Then, if the number of possible solutions for $\boldsymbol{\phi}$ is limited and is not too large, some coarse partial channels $\widetilde{\mathbf{H}}$ and $\widetilde{\mathbf{G}}$ obtained from fewer active antennas can be utilized to establish a well mapping between these partial channels and an optimal beamforming vector $\boldsymbol{\phi}^s$ in $\mathcal{B}$. Note that the selection of the activation pattern $\mathcal{M}$ would also greatly impact the performance of the mapping. We propose a DL-based beam searching scheme to optimize the activation pattern $\mathcal{M}$ and to extract the hidden relationship between the partial channels and the optimal beamforming vector in $\mathcal{B}$. The overall flow of the designed scheme is expressed as

$$\{\mathbf{H}, \mathbf{G}\} \xrightarrow{\text{spatial sub-sampling}} \{\widetilde{\mathbf{H}}, \widetilde{\mathbf{G}}\} \xrightarrow{\text{beam searching}} \{\boldsymbol{\phi}^s\}. \quad (31)$$

Similar to the channel extrapolation scheme, the beam searching scheme also contains two main parts, i.e., the active antenna selection network and the beam searching network, to separately conduct the spatial sub-sampling operation and the beam searching operation in (31).

A. Active Antenna Selection Network

Since the structure of the active antenna selection network in the beam searching scheme is similar to that in the channel extrapolation scheme in Fig. 3, we omit the description of this part and directly propose the beam searching network in the following part.

This article has been accepted for publication in a future issue of this journal, but has not been fully edited. Content may change prior to final publication. Citation information: DOI 10.1109/TCOMM.2021.3097726, IEEE Transactions on Communications

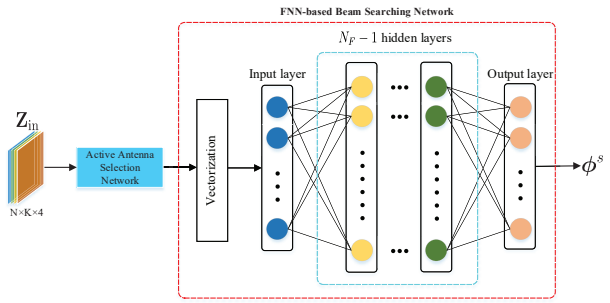

Fig. 5. The structure of the proposed beam searching network.

TABLE II
THE STRUCTURE OF THE FNN-BASED BEAM SEARCHING NETWORK.

Name	Parameter
Number of hidden layers	N_F-1
Number of output nodes in the l-th hidden layer	N_l
Activation functions for hidden layers	Leaky ReLU
Activation function for output layer	Softmax

B. Beam Searching Network

The beam searching network aims to find an optimal beamforming vector $\boldsymbol{\phi}^s$ in the codebook $\mathcal{B}$ with given $\widetilde{\mathbf{H}}$ and $\widetilde{\mathbf{G}}$. Compared with the CNN-based channel extrapolation network that requires relatively expensive training overhead, the output dimension of the beam searching network is much lower. This inspires us to adopt FNN for the beam searching network to find out the optimal beamforming vector $\boldsymbol{\phi}^s$, as shown in Fig. 5. We use the codebook $\mathcal{B}$ to construct the training target so that once the beam searching network is fed with an input $\bar{\mathbf{Z}}$, it can pick up one $\boldsymbol{\phi}^s$ from $\mathcal{B}$ to maximize the achievable rate R. Since the training of the active antenna selection network and the beam searching network are implemented jointly, the corresponding index for $\boldsymbol{\phi}^s$ in $\mathcal{B}$ can be viewed as a label attached to a specific full channel pair $\{\mathbf{H}, \mathbf{G}\}$, i.e., the input data $\mathbf{Z}_{\text{in}}$ of the active antenna selection network in the beam searching scheme. Hence, the expected output of the beam searching network can be transformed into $\mathbf{p}^s$, a one-hot encoding vector of size $|\mathcal{B}| \times 1$, and the index of the non-zero element in $\mathbf{p}^s$ indicates the location of $\boldsymbol{\phi}^s$ in $\mathcal{B}$.

We adopt the FNN-based beam searching network to obtain the optimal beamforming as

$$\widehat{\mathbf{p}^s} = G_{\mathcal{W}_B}(\bar{\mathbf{Z}}), \tag{32}$$

where $\mathcal{W}_B$ represents the trainable parameters set of the FNN-based beam searching network, while $\widehat{\mathbf{p}^s}$ represents the output of the beam searching network and includes the corresponding probabilities for all classifications with respect to the input data $\mathbf{Z}_{\text{in}}$. Then, the index of the maximum value in $\widehat{\mathbf{p}^s}$ is the estimated location of $\boldsymbol{\phi}^s$ in $\mathcal{B}$.

Similar to the channel extrapolation, we list the corresponding network structure in TABLE II. Note that in the beam searching network, the input $\bar{\mathbf{Z}}$ is first flatten into a vector to the input layer and is then fully-connected with the subsequent hidden layer. The dropout operation is utilized for all but the last hidden layer to avoid overfitting [52]. The details about the values of the parameters in TABLE II can be found in Section V. Correspondingly, the feasibility of the beam searching is presented in Appendix C.

C. Training and Deployment for Active Antenna Selection and Beam Searching Networks

Similar to Section III-C, during the off-line training phase for both active antenna selection and beam searching networks, we first set $\mathbb{R}$ as fully-active to collect the channels at the RIS's elements and further construct the label samples for the off-line training of the network. We use the available full channel data pair $\{\mathbf{H}, \mathbf{G}\}$ and the per-defined codebook $\mathcal{B}$ to get the corresponding label $\mathbf{p}^s$. A sample in the training set $\mathcal{D}$ is denoted by $(\mathbf{Z}_{\text{in}}, \mathbf{p}^s)$, where the input data $\mathbf{Z}_{\text{in}}$ for the beam searching scheme has the same definition as that for the channel extrapolation scheme in (10). The categorical cross entropy between the output and label is used as the loss function of the beam searching network, which can be expressed as

$$\mathcal{L}_b = -\frac{1}{M_{tr}} \sum_{\mu=0}^{M_{tr}-1} \sum_{i=0}^{|\mathcal{B}|-1} p_i^{\mu} \log \widehat{p}_i^{\mu}, \tag{33}$$

where p_i and $\widehat{p}_i$ are separately the i-th element in $\mathbf{p}^s$ and $\widehat{\mathbf{p}^s}$, and M_{tr} is the batch size for network training.

Considering the loss of the active antenna selection network in (21), the resultant optimization problem for the beam searching scheme is denoted as

$$\left\{\widehat{\mathcal{W}}_B, \widehat{\boldsymbol{\Xi}}\right\} = \arg \min_{\mathcal{W}_B, \boldsymbol{\Xi}} (\mathcal{L}_b + \rho \mathcal{L}_s), \tag{34}$$

where $\mathcal{L}_B \triangleq \mathcal{L}_b + \rho \mathcal{L}_s$ is the training loss of the beam searching scheme.

During the off-line training phase, the Adam optimizer is adopted to achieve the optimal model parameters $\widehat{\mathcal{W}}_B$ and $\widehat{\boldsymbol{\Xi}}$. Since the off-line training for the beam searching network is similar with that for the channel extrapolation network, we omit some description due to space limitation. More details about the training of the beam searching network are specified in Section V.

After completing the off-line training, the optimal activation pattern $\mathcal{M}$ can be acquired from the trained active antenna selection network, and the optimal locations of the active antenna elements are determined. Then, we adjust $\mathbb{R}$ from the fully-active model to the semi-active one, where only a small fraction of the reflection elements are active.

In the subsequent on-line deployment phase, once $\mathbb{R}$ obtains the partial channels $\widetilde{\mathbf{H}}$ and $\widetilde{\mathbf{G}}$ from the channel estimation stage, it can directly determine the optimal beamforming vector $\boldsymbol{\phi}^s$ in the codebook $\mathcal{B}$ and further utilize the corresponding phase shift vector $\boldsymbol{\theta}^s$ to assist the communication between $\mathbb{S}$ and $\mathbb{D}$ during the data transmission stage.

V. SIMULATION RESULTS

In this section, we evaluate the performance of the designed channel extrapolation scheme and beam searching scheme through numerical simulations.

This article has been accepted for publication in a future issue of this journal, but has not been fully edited. Content may change prior to final publication. Citation information: DOI 10.1109/TCOMM.2021.3097726, IEEE Transactions on Communications

TABLE III
THE ADOPTED DEEPMIMO DATASET PARAMETERS.

Parameter	value
Name of scenario	I1
The carrier frequency of channel estimation and data transmission	2.4 GHz, 2.5 GHz
Number of BS antennas in (x, y, z)	(8, 8, 1)
Number of paths	5
Active users as the transmitters $\mathbb{S}$	Row 1 to 200
Active users as the transmitters $\mathbb{D}$	Row 201 to 400
System bandwidth	100 MHz
Number of selected OFDM sub-carriers	64

TABLE V
LAYER PARAMETERS FOR THE FNN-BASED BEAM SEARCHING NETWORK.

Layer	Output size	Activation
Flatten	16384	-
FNN 1	16384	Leaky ReLU ($\alpha = 0.2$)
Dropout 1 (50%)	16384	-
FNN 2	4096	Leaky ReLU ($\alpha = 0.2$)
Dropout 2 (50%)	4096	-
FNN 3	4096	Leaky ReLU ($\alpha = 0.2$)
Dropout 3 (50%)	4096	-
FNN 4	2048	Leaky ReLU ($\alpha = 0.2$)
FNN 5	256	Softmax

A. Communication Scenario and DeepMIMO Dataset

In order to make full use of the spatial correlation and spatial consistency hidden in the channel dataset, it is reasonable to adopt a realistic electromagnetic environment for generating the channels. Thus, we resort to the indoor massive MIMO scenario 'I1' of the DeepMIMO dataset [48], which is generated based on the Wireless InSite [53] and is widely used in DL applications for massive MIMO systems.

The primary parameters for simulation are listed in TABLE III. We adopt the BS 8 in the 'I1' scenario as $\mathbb{R}$ for the considered system model and set it as an UPA with 8×8 ($N = 64$) antennas. In the frequency division duplex operation, the forward link $\mathbb{S} \to \mathbb{R} \to \mathbb{D}$ and the backward link $\mathbb{D} \to \mathbb{R} \to \mathbb{S}$ work in different frequency bands. Intuitively, different activation patterns $\mathcal{M}$ could be selected at different frequency bands for the forward and the backward links, respectively. However, this solution would increase the system's power consumption and decrease its spectral efficiency. A feasible method is that the two links share the same activated RIS elements from one frequency band. Thus, there exists frequency mismatch between the estimated channels and the channels to be extrapolated. To exhibit the ability of channel extrapolation between different frequencies, we set the carrier frequencies for the channel estimation stage and the data transmission stage as $f_a = 2.4$ GHz and $f_c = 2.5$ GHz, respectively. Denote $\mathbf{H}^a$ and $\mathbf{G}^a$ as the channel matrices with carrier frequency f_a. For UPA, the antenna spacing d is set to $\frac{\lambda_c}{2}$ and $\frac{\lambda_c}{4}$, respectively. Moreover, we select the users located within the regions from the 1st row to the 200th row and from the 201th row to the 400th row in the 'I1' scenario as the transmitters $\mathbb{S}$ and receivers $\mathbb{D}$, respectively. Since each row in the aforementioned regions contains 201 users, the total number of users is 80400. We select each $\mathbb{S}$-$\mathbb{D}$ pair from their corresponding regions to further generate 40200 samples. The bandwidth of the OFDM system is set as 100 MHz and the number of OFDM sub-carriers is 1024 for the entire bandwidth. However, to reduce the size of the generated channels and save the memory, we select the channels at the first $K = 64$ sub-carriers. The channels $\mathbf{H}^a$, $\mathbf{G}^a$, $\mathbf{H}$ and $\mathbf{G}$ are generated from the DeepMIMO dataset [48]. Typically, we adopt $\mathbf{C}_{N_v,r_1} \otimes \mathbf{C}_{N_h,r_2}$ as the beamforming codebook $\mathcal{B}$ to match the structure of the proposed RIS, where $\mathbf{C}_{N_v,r_1} \in \mathcal{C}^{N_v \times r_1 N_v}$ and $\mathbf{C}_{N_h,r_2} \in \mathcal{C}^{N_h \times r_2 N_h}$ are separately the beamforming codebooks along the vertical and horizontal dimensions, while r_1 and r_2 are the over-sampling coefficients for $\mathbf{C}_{N_v,r_1}$ and $\mathbf{C}_{N_h,r_2}$, respectively. The (i,j)-th entry of $\mathbf{C}_{N_v,r_1}$ is defined as $[\mathbf{C}_{N_v,r_1}]_{i,j} = e^{-\jmath \frac{2\pi}{r_1 N_v} ij}, i = 0, 1, \cdots, N_v - 1, j = 0, 1, \cdots, r_1 N_v - 1$ and the entries in $\mathbf{C}_{N_h,r_2}$ have a similar definition.

B. Network Parameter Configuration

In the channel extrapolation scheme, one sample of the dataset is composed of two channel sets $\{\mathbf{H}^a, \mathbf{G}^a\}$ and $\{\mathbf{H}, \mathbf{G}\}$. We employ 80% of the dataset for network training and the rest for testing. Considering the CNN-based channel extrapolation network, we use 3×3 convolutional kernels and set $P = 1$ and $S = 1$ for all convolutional layers. Specially, we set $N_p = 5$ and $N_q = 6$ to learn a powerful proximal operator as shown in Fig. 4. The initial parameters for the learning rates are set as $\eta_\xi = 1e-3$ and $\eta_\omega = 1e-4$, respectively, and the penalty multiplier ρ is taken as $1e-4$. The Adam optimizer is used for the network training with batch size 16. We conduct the training of the active antenna selection network and the channel extrapolation network until the training loss converges. TABLE IV provides the layer parameters of the channel extrapolation network.

For the beam searching scheme, the input data is the same as that for the channel extrapolation scheme. We set the over-sampling coefficients for the codebook $\mathcal{B}$ as $r_1 = r_2 = 2$. Each label $\mathbf{p}^s$ in a sample of the training dataset corresponds to an optimal beamforming vector $\boldsymbol{\phi}^s$ searched in $\mathcal{B}$. The dataset is divided with the same ratio as that for the channel extrapolation scheme. We adopt four hidden layers for the FNN-based beam searching network. The initial learning rates are $\eta_\xi = 1e-2$ and $\eta_\omega = 1e-4$, respectively, and the penalty multiplier ρ is $1e-4$. The Adam optimizer is used for the network training with batch size 256 and the epoch for training is set to 500. The layer parameters of the beam searching network are listed in TABLE V.

C. Performance Evaluation

The baseline scheme for comparison is the uniform selection strategy adopted in [46]. Note that the curves labeled by 'Unif' correspond to the active antenna selection network with uniform selection strategy, while the ones marked by 'Prob'

This article has been accepted for publication in a future issue of this journal, but has not been fully edited. Content may change prior to final publication. Citation information: DOI 10.1109/TCOMM.2021.3097726, IEEE Transactions on Communications

TABLE IV
LAYER PARAMETERS FOR THE CNN-BASED CHANNEL EXTRAPOLATION NETWORK.

Layer	Output size	Activation	Kernel size	Strides
1× Conv2D	$64 \times 64 \times 4$	None	3×3	1×1
6× Conv2D (proximal-gradient iteration)	$64 \times 64 \times 64$	ReLU	3×3	1×1
1× Conv2D (proximal-gradient iteration)	$64 \times 64 \times 4$	None	3×3	1×1
1× Conv2D (proximal-gradient iteration)	$64 \times 64 \times 4$	None	3×3	1×1

represent the performance of the active antenna selection network with the proposed probabilistic selection strategy. Fig. 6 depicts the normalized MSE (NMSE) for the channel extrapolation scheme versus the spatial compression ratio r. It

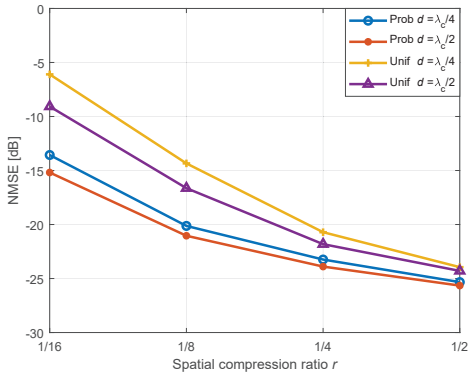

Fig. 6. The NMSE of channel extrapolation versus the spatial compression ratio r.

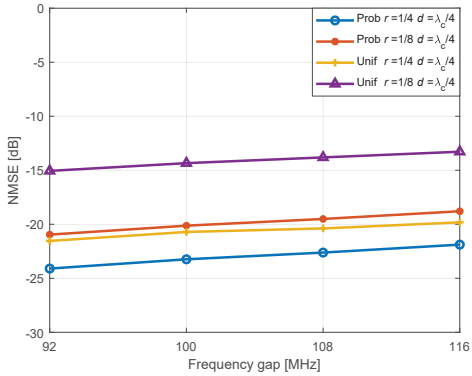

Fig. 7. The NMSE of channel extrapolation versus frequency gaps.

can be seen that all NMSE curves decrease with the increase of r, where $r \in \{\frac{1}{16}, \frac{1}{8}, \frac{1}{4}, \frac{1}{2}\}$. Moreover, it can be found that the performance of the proposed channel extrapolation scheme with probabilistic selection strategy is better than that with uniform selection strategy for both $d = \frac{\lambda_c}{4}$ and $d = \frac{\lambda_c}{2}$. Furthermore, compared with the case of $d = \frac{\lambda_c}{4}$, the proposed scheme with $d = \frac{\lambda_c}{2}$ can obtain a better performance. This is because a smaller antenna spacing leads to a higher correlation between the channels of neighboring antennas that can not be distinguished, which reduces the channel variation among the sampled antennas and damages the CNN's extrapolation performance.

In Fig. 7, we respectively extract the channels of 4 neighbouring subcarriers from $\{\mathbf{H}^a, \mathbf{G}^a\}$ and $\{\mathbf{H}, \mathbf{G}\}$ and evaluate the NMSE performance of the channel extrapolation scheme versus the subcarrier frequency gaps between channel matrices, where four different frequency gaps are considered, with $d = \frac{\lambda_c}{4}$. It can be found that as the subcarrier frequency gap increases, the NMSE gradually increases. However, the performance impact is not large, which means that the proposed scheme can achieve a good extrapolation performance even with larger frequency gap. Furthermore, with the same r, the performance of the proposed scheme with the probabilistic selection strategy is always better than that with the uniform selection strategy, which verifies its effectiveness.

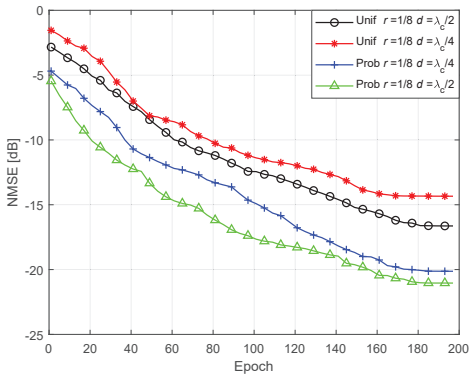

Fig. 8. The NMSE of channel extrapolation versus epochs.

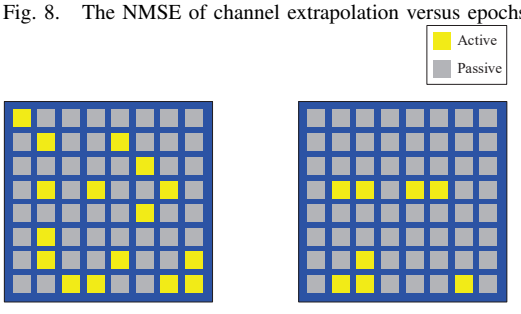

Fig. 9. (a) The active antenna selection under $r = 1/4$. (b) The active antenna selection under $r = 1/8$.

Fig. 8 shows the NMSE performance of the channel extrapolation scheme with probabilistic and uniform selection strategy versus epoch for network training, with $r = \frac{1}{8}$. It can be seen that the NMSE decreases with the epoch. Additionally, it is worth mentioning that during the training, the performance of the probabilistic selection strategy is always better than that of the uniform selection strategy, which proves the gain of the antenna selection network.

This article has been accepted for publication in a future issue of this journal, but has not been fully edited. Content may change prior to final publication. Citation information: DOI 10.1109/TCOMM.2021.3097726, IEEE Transactions on Communications

Fig. 9 displays the active antenna selection results of $r = \frac{1}{4}$ and $r = \frac{1}{8}$, with $d = \frac{\lambda_c}{2}$. It can be found that there are 16 non-uniform active antennas selected under $r = \frac{1}{4}$ and 8 non-uniform active antennas selected under $r = \frac{1}{8}$. Moreover, from the two sub-figures, it can be found that the uniform selection strategy is not optimal and the probabilistic selection strategy can achieve a better performance, which shows the effectiveness of the proposed probabilistic active antenna selection network.

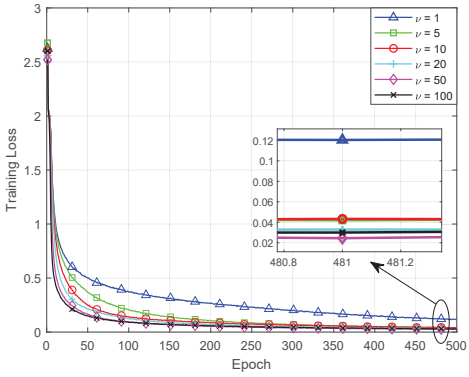

Fig. 10. Training loss with different learning rate ratio for probabilistic selection.

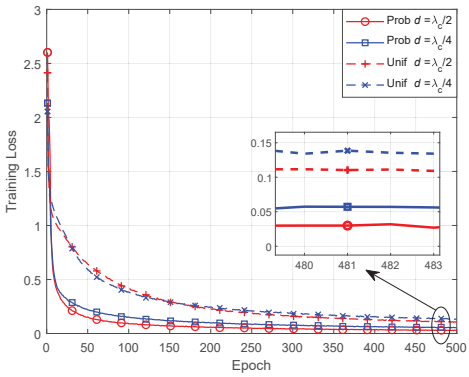

Fig. 11. Training loss with different selection strategies and antenna spacings.

Fig. 10 presents the training loss versus the epoch of the beam searching scheme with probabilistic selection strategy, where different learning rate ratio $\nu = \frac{\eta_\xi}{\eta_\omega}$ is considered and $r = \frac{1}{8}$. It can be seen that the training loss decreases with the epoch. Besides, when $\nu \leq 50$, it can be noticed that the larger the learning rate ratio is, the lower the training loss is. This is because a larger learning rate ratio can accelerate the training of the selection network. However, we can see that the rate of convergence of the training loss is approaching a limit when $\nu = 100$. It means that when $\nu > 100$, increasing ν has limited benefit to the classification performance of the beam searching network.

In Fig. 11, we set $\nu = 50$ and $r = \frac{1}{8}$, with which a faster training loss convergence can be achieved as proved in Fig. 10. The figure shows the comparison of the training loss for the beam searching scheme with d set as $\frac{\lambda_c}{2}$ and $\frac{\lambda_c}{4}$, respectively. It can be seen that the performance with $d = \frac{\lambda_c}{2}$ is better than that with $d = \frac{\lambda_c}{4}$, which confirms the explanation provided for the results in Fig. 6. In addition, Fig. 11 also presents the performance comparison between the uniform selection strategy and the probabilistic selection strategy, which verifies the considerable gain of the proposed probabilistic selection strategy.

Fig. 12 shows the performance comparison for different r values, for the beam searching scheme with the probabilistic and uniform selection strategy, respectively. It can be found that the performance enhances with the increase of r. Besides, for each r, the probabilistic selection strategy always provides a performance gain compared with the uniform selection strategy. It is worth noting that when the spatial compression ratio becomes large enough, i.e., $r = \frac{1}{4}$, the probabilistic selection strategy shows a limited performance gain compared with the uniform selection strategy. This is because when the number of sampled elements increases, the sampling strategy have less impact on the classification performance of the subsequent beam searching network.

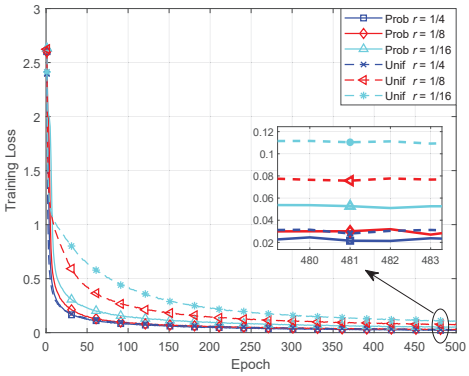

Fig. 12. Training loss with different selection strategies and spatial compression ratios.

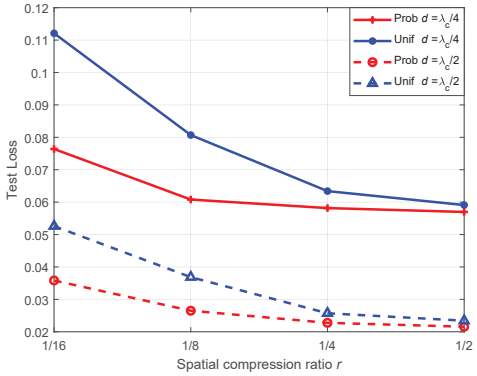

Fig. 13. Test loss versus spatial compression ratios with different selection strategies and antenna spacings.

In Fig. 13, the classification performance on the test set is depicted versus the spatial compression ratio for the beam searching scheme, where both probabilistic and uniform selection strategy with two different antenna spacings are considered. Results show that the test loss decreases with increasing r for both selection strategies. Moreover, Fig. 13 illustrates the significant gain of the probabilistic selection strategy at

This article has been accepted for publication in a future issue of this journal, but has not been fully edited. Content may change prior to final publication. Citation information: DOI 10.1109/TCOMM.2021.3097726, IEEE Transactions on Communications

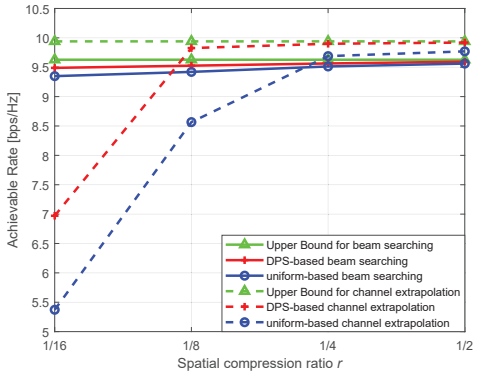

Fig. 14. Achievable rate versus spatial compression ratio with different selection strategies for the channel extrapolation scheme and the beam searching scheme, with $d = \frac{\lambda_c}{2}$.

a lower spatial compression ratio, i.e., $r = \frac{1}{16}$ and $r = \frac{1}{8}$, compared with the uniform selection strategy. In addition, the gap between the test loss of probabilistic and uniform selection strategies reduces as r increases. Especially, when $r = \frac{1}{2}$, the test loss of probabilistic and uniform selection strategies are very close, for both $d = \frac{\lambda_c}{2}$ and $d = \frac{\lambda_c}{4}$, respectively, which has been explained in the description of Fig. 12.

Fig. 14 shows the comparison of the achievable rate for the two proposed schemes when $d = \frac{\lambda_c}{2}$ and the SNR is 30 dB. Note that the upper bound for the channel extrapolation scheme is defined as the maximum achievable rate with the perfect individual CSI, which can be derived by substituting the optimal beamforming vector $\boldsymbol{\phi}^{\diamond}$ in (29) and SNR into (4). The upper bound for the beam searching scheme is defined as the maximum achievable rate with the optimal beamforming vector $\boldsymbol{\phi}^{s}$ in codebook $\mathcal{B}$, which can be derived by substituting $\boldsymbol{\phi}^{s}$ and SNR into (4). It can be seen that due to the limitation of the designed codebook $\mathcal{B}$, the upper bound of the achievable rate for the beam searching scheme is lower than that for the channel extrapolation scheme. Moreover, since the optimal beamforming vector in (29) highly depends on the performance of channel extrapolation, the achievable rate is lower for the channel extrapolation scheme compared with the beam searching scheme when $r = \frac{1}{16}$. It can be seen that the achievable rate for the beam searching scheme is stable when r reduces. This demonstrates the robustness of the proposed beam searching scheme, which requires fewer active elements to obtain a considerable rate. Furthermore, when r increases, the achievable rate for the channel extrapolation scheme becomes higher than that for the beam searching scheme. This can be explained that the performance of the channel extrapolation is greatly improved when r increases, and a better beamforming vector can be found based on (29) compared with the codebook $\mathcal{B}$. For both the beam searching scheme and the channel extrapolation scheme, the achievable rate with the probabilistic selection strategy is higher than that with the uniform selection strategy, which again verifies the gain of the probabilistic sampling compared with the uniform sampling.

VI. Conclusion

In this paper, we have examined the active element-aided RIS communication system and proposed two DL-based schemes, i.e., the channel extrapolation scheme and the beam searching scheme. For both schemes, the probabilistic sampling theory has been utilized to find the optimal locations of the active RIS elements. Moreover, a CNN-based channel extrapolation network has been designed to extrapolate the full channels from the estimated partial channels in the channel extrapolation scheme. On the other hand, an FNN-based beam searching network has been designed to achieve the direct mapping from the estimated partial channels to the optimal beamforming vector in the beam searching scheme. The efficient BP has been utilized to optimize the proposed networks during training. Simulation results have illustrated that the proposed optimal antenna selection is superior to the uniform antenna selection, and the beam searching scheme is more robust than the channel extrapolation scheme with fewer active antennas. The extension to the multiuser-MIMO case can be considered as part of future work.

Appendix A
A Property of the Gumbel Noise

The detailed reason for using the Gumbel distribution can be explained as follows. It can be proved that if we perturb the logit $\xi_{m,n}$ with Gumbel noise $w_{m,n}$, the underlying distribution from which we sample still exactly matches the normalized probability in (13).

Proof: The Gumbel distribution with unit scale and location parameter μ, i.e., $\mathrm{Gumebl}(\mu, 1)$, has the following probability density function

$$f(z;\mu) = \exp\{-(z-\mu) - \exp\{-(z-\mu)\}\}. \tag{36}$$

The cumulative probability function of the Gumbel is

$$F(z;\mu) = \exp\{-\exp\{-(z-\mu)\}\}. \tag{37}$$

Note that in the following part we ignore the subscript m for simplicity. Define $z_n = \xi_n + w_n$. From $w_n \sim \mathrm{Gumbel}(0,1)$, we have $z_n \sim \mathrm{Gumbel}(\xi_n, 1)$. Correspondingly, the probability that all other $z_{n' \neq n}$ are less than z_n is

$$\begin{aligned}
&P(z_n \geq z_{n'}; \forall n' \neq n | z_n, \{\xi_{n'}\}_{n'=0}^{N-1}) \\
=&P(z_0 \leq z_n)P(z_1 \leq z_n)\cdots P(z_{n-1} \leq z_n)P(z_{n+1} \leq z_n) \\
&\cdots P(z_{N-1} \leq z_n) \\
=&F(z_n;\xi_0)F(z_n;\xi_1)\cdots F(z_n;\xi_{n-1})F(z_n;\xi_{n+1}) \\
&\cdots F(z_n;\xi_{N-1}) \\
=&\prod_{n' \neq n} F(z_n;\xi_{n'}) \\
=&\prod_{n' \neq n} \exp\{-\exp\{-(z_n - \xi_{n'})\}\}.
\end{aligned} \tag{38}$$

To obtain the marginal distribution over z_n, we need to integrate it out to find the overall probability as (35) on the top of the next page, where $(*)$ in (35) shows an integral over a Gumbel distribution with the location parameter

This article has been accepted for publication in a future issue of this journal, but has not been fully edited. Content may change prior to final publication. Citation information: DOI 10.1109/TCOMM.2021.3097726, IEEE Transactions on Communications

$$
\begin{aligned}
&P\left(z_n \geq z_{n'}; \forall n' \neq n \middle| \{\xi_{n'}\}_{n'=0}^{N-1}\right) \\
&= \int f(z_n;\xi_n) \cdot P(z_n \geq z_{n'}; \forall n' \neq n | z_n, \{\xi_{n'}\}_{n'=0}^{N-1}) dz_n \\
&= \int \exp\{-(z_n-\xi_n) - \exp\{-(z_n-\xi_n)\}\} \cdot \prod_{n' \neq n} \exp\{-\exp\{-(z_n-\xi_{n'})\}\} dz_n \\
&= \int \exp\{-(z_n-\xi_n)\} \cdot \prod_{n'=0}^{N-1} \exp\{-\exp\{-(z_n-\xi_{n'})\}\} dz_n \\
&= \int \exp\left\{-\exp\{-z_n\} \sum_{n'=0}^{N-1} \exp\{\xi_{n'}\} - z_n + \xi_n\right\} dz_n \\
&= \int \exp\left\{-\exp\left\{-z_n + \ln\left(\sum_{n'=0}^{N-1} \exp\{\xi_{n'}\}\right)\right\} - z_n + \xi_n\right\} dz_n \\
&= \exp\left\{-\ln\left(\sum_{n'=0}^{N-1} \exp\{\xi_{n'}\}\right) + \xi_n\right\} \cdot \int \exp\left\{-\exp\left\{-z_n + \ln\left(\sum_{n'=0}^{N-1} \exp\{\xi_{n'}\}\right)\right\} - \left(z_n - \ln\left(\sum_{n'=0}^{N-1} \exp\{\xi_{n'}\}\right)\right)\right\} dz_n \\
&= \frac{\exp\{\xi_n\}}{\sum_{n'=0}^{N-1} \exp\{\xi_{n'}\}} \cdot \underbrace{\int \exp\left\{-\left(z_n - \ln\left(\sum_{n'=0}^{N-1} \exp\{\xi_{n'}\}\right)\right) - \exp\left\{-\left(z_n - \ln\left(\sum_{n'=0}^{N-1} \exp\{\xi_{n'}\}\right)\right)\right\}\right\} dz_n}_{(*)},
\end{aligned} \tag{35}
$$

$\mu = \ln(\sum_{n'=0}^{N-1} \exp\{\xi_{n'}\})$ and is equal to 1. Thus, we have

$$
P(z_n \geq z_{n'}; \forall n' \neq n | \{\xi_{n'}\}_{n'=0}^{N-1}) = \frac{\exp\{\xi_n\}}{\sum_{n'=0}^{N-1} \exp\{\xi_{n'}\}}, \tag{39}
$$

which is exactly the normalized probability in (13). ∎

From the above proof, we can obtain the fact that adding Gumbel noise does not change the original distribution, which is a specific property of the Gumbel noise.

Appendix B
Feasibility of Channel Extrapolation

From (2), we define the parameter set for $\mathbf{H}$ as $\mathcal{Q}_h(f_c) = \{h_{p,f_c}, \tau_{h,p}, \phi_{h,p}, \varphi_{h,p}\}_{p=1}^{P_h}$. With the fixed structure of $\mathbb{R}$, $\mathbf{H}$ can be derived from $\mathcal{Q}_h(f_c)$. Thus, $\mathcal{Q}_h(f_c)$ can be seen as the physical intrinsic factor of the link along $\mathbb{S} \to \mathbb{R}$. Before proceeding, we give the following definitions:

Definition 1: The mapping function $\mathbf{\Phi}_{\mathcal{N},f_c}$ from the physical intrinsic factor set $\mathcal{Q}_h(f_c)$ to the channel $\mathbf{H}$ can be written as

$$
\mathbf{\Phi}_{\mathcal{N},f_c} : \{\mathcal{Q}_h(f_c)\} \to \{\mathbf{H}\}, \tag{40}
$$

where the sets $\{\mathcal{Q}_h(f_c)\}$ and $\{\mathbf{H}\}$ are the domain and codomain of $\mathbf{\Phi}_{\mathcal{N},f_c}$, respectively.

Under the fixed scattering scenario, if the number of RIS elements is large enough, we can extract $\mathcal{Q}_h(f_c)$ from $\mathbf{H}$, which can be easily checked from (2). With the physical meanings of $\mathcal{Q}_h(f_c)$, we have the following bijective mapping [44] relation

$$
\mathcal{Q}_h(f_c) \leftrightarrow \mathbf{H}. \tag{41}
$$

Thus, the above defined mapping function (40) is bijective, which means that $\mathcal{Q}_h(f_c)$ corresponds to a unique channel $\mathbf{H}$, and vice versa. Then, the inverse mapping of $\mathbf{\Phi}_{\mathcal{N},f_c}$ exists and can be expressed as

$$
\mathbf{\Phi}_{\mathcal{N},f_c}^{-1} : \{\mathbf{H}\} \to \{\mathcal{Q}_h(f_c)\}. \tag{42}
$$

Definition 2: The mapping function $\mathbf{\Phi}_{\mathcal{M},f_c}$ from $\mathcal{Q}_h(f_c)$ to the partial channel $\widetilde{\mathbf{H}}$ can be denoted as

$$
\mathbf{\Phi}_{\mathcal{M},f_c} : \{\mathcal{Q}_h(f_c)\} \to \{\widetilde{\mathbf{H}}\}, \tag{43}
$$

where the sets $\{\mathcal{Q}_h(f_c)\}$ and $\{\widetilde{\mathbf{H}}\}$ are the domain and codomain of $\mathbf{\Phi}_{\mathcal{M},f_c}$, respectively.

Since $\mathcal{M}$ is a subset of $\mathcal{N}$ and $\widetilde{\mathbf{H}}$ is formed by the elements in $\mathbf{H}$, with the results in Definition 1, it can be determined that the mapping function (43) is bijective when the elements in $\mathcal{M}$ are sufficient. Correspondingly, the inverse mapping of $\mathbf{\Phi}_{\mathcal{M},f_c}$ is

$$
\mathbf{\Phi}_{\mathcal{M},f_c}^{-1} : \{\widetilde{\mathbf{H}}\} \to \{\mathcal{Q}_h(f_c)\}. \tag{44}
$$

With the bijective properties of the mapping functions in (40) and (43), we can obtain the following proposition.

Proposition 1 [44]: For the given communication environment and RIS structure, the mapping relation from the partial channel $\widetilde{\mathbf{H}}$ to the full channel $\mathbf{H}$ can be characterized by the function $\mathbf{\Psi}_{\mathcal{M},f_c \to \mathcal{N},f_c}$ defined as

$$
\mathbf{\Psi}_{\mathcal{M},f_c \to \mathcal{N},f_c} = \mathbf{\Phi}_{\mathcal{N},f_c} \circ \mathbf{\Phi}_{\mathcal{M},f_c}^{-1} : \{\widetilde{\mathbf{H}}\} \to \{\mathbf{H}\}, \tag{45}
$$

where $\circ$ denotes the composite mapping operation.

The above proposition demonstrates that the extrapolation of $\mathbf{H}$ from $\widetilde{\mathbf{H}}$ is feasible. We can consider a similar process for $\mathbf{G}$ and $\widetilde{\mathbf{G}}$ and verify the feasibility of the proposed channel extrapolation [54]. Then, with feasible mapping between the partial channels and the full channels, we can effectively recover $\mathbf{H}$ and $\mathbf{G}$ from $\widetilde{\mathbf{H}}$ and $\widetilde{\mathbf{G}}$, respectively.

APPENDIX C
FEASIBILITY OF BEAM SEARCHING

Within the beam searching scheme, the optimal beamforming vector $\boldsymbol{\phi}^s$ at $\mathbb{R}$ is chosen from the codebook $\mathcal{B}$. Since the feasible mapping from the partial channels $\widetilde{\mathbf{H}}$ and $\widetilde{\mathbf{G}}$ to the full channels $\mathbf{H}$ and $\mathbf{G}$ exists, with the extrapolated $\mathbf{H}$ and $\mathbf{G}$, we can traverse all possible vectors in $\mathcal{B}$ and find the optimal beamforming vector $\boldsymbol{\phi}^s$ by utilizing (4) as performance metric. Obviously, one set $\{\mathbf{H}, \mathbf{G}\}$ corresponds to only one determined $\boldsymbol{\phi}^s$. Hence, there exists explicit mapping between $\{\widetilde{\mathbf{H}}, \widetilde{\mathbf{G}}\}$ and $\boldsymbol{\phi}^s$ within $\mathcal{B}$. Accordingly, the beam searching is also feasible. For clarity, we give the following proposition.

Proposition 2: If $\boldsymbol{\phi}$ is selected from $\mathcal{B}$, then there exists a specific mapping relation from $\{\widetilde{\mathbf{H}}, \widetilde{\mathbf{G}}\}$ to the optimal $\boldsymbol{\phi}^s$. Correspondingly, this mapping is expressed as

$$\boldsymbol{\Pi}_{\mathcal{M}\to\mathcal{B}} : \left\{\widetilde{\mathbf{H}}, \widetilde{\mathbf{G}}\right\} \to \{\boldsymbol{\phi}^s\}. \tag{46}$$

REFERENCES

[1] C. Huang *et al.*, "Holographic MIMO surfaces for 6G wireless networks: Opportunities, challenges, and trends," *IEEE Wireless Commun.*, vol. 27, no. 5, pp. 118–125, Oct. 2020.

[2] N. Rajatheva *et al.*, "White paper on broadband connectivity in 6g," arXiv:2004.14247v1, 2020. [Online]. Available: https://arxiv.org/abs/2004.14247v1.

[3] N. Rajatheva *et al.*, "Scoring the terabit/s goal: Broadband connectivity in 6g," arXiv:2008.07220v1, 2020. [Online]. Available: https://arxiv.org/abs/2008.07220v1.

[4] E. Basar *et al.*, "Wireless communications through reconfigurable intelligent surfaces," *IEEE Access.*, vol. 7, pp. 116753–116773, Sept. 2019.

[5] X. Guan, Q. Wu, and R. Zhang, "Intelligent reflecting surface assisted secrecy communication: is artificial noise helpful or not?," *IEEE Commun. Lett.*, vol. 9, no. 6, pp. 778–782, Jun. 2020.

[6] B. Di, H. Zhang, L. Song, Y. Li, Z. Han, and H. V. Poor, "Hybrid beamforming for reconfigurable intelligent surface based multi-user communications: achievable rates with limited discrete phase shifts," *IEEE J. Sel. Areas Commun.*, vol. 38, no. 8, pp. 1809–1822, Aug. 2020.

[7] X. Hu, C. Zhong, Y. Zhang, X. Chen, and Z. Zhang, "Location information aided multiple intelligent reflecting surface systems," *IEEE Trans. Commun.*, vol. 68, no. 12, pp. 7948–7962, Dec. 2020.

[8] S. Lin, B. Zheng, G. C. Alexandropoulos, M. Wen, F. Chen, and S. Mumtaz, "Adaptive transmission for reconfigurable intelligent surface-assisted OFDM wireless communications," *IEEE J. Sel. Areas Commun.*, vol. 38, no. 11, pp. 2653–2665, Nov. 2020.

[9] M. Zeng, X. Li, G. Li, W. Hao, and O. A. Dobre, "Sum rate maximization for IRS-assisted uplink NOMA," *IEEE Commun. Lett.*, vol. 25, no. 1, pp. 234–238, Jan. 2021.

[10] J. Zuo, Y. Liu, E. Basar, and O. A. Dobre, "Intelligent reflecting surface enhanced millimeter-wave NOMA systems," *IEEE Commun. Lett.*, vol. 24, no. 11, pp. 2632–2636, Nov. 2020.

[11] Q. Wu and R. Zhang, "Intelligent reflecting surface enhanced wireless network: joint active and passive beamforming design," in *Proc. IEEE Global Communication Conference (GLOBECOM),* Dec. 2018, pp. 1–6.

[12] W. Tang *et al.*, "MIMO transmission through reconfigurable intelligent surface: system design, analysis, and implementation," *IEEE J. Sel. Areas Commun.*, vol. 38, no. 11, pp. 2683–2699, Nov. 2020.

[13] X. Hu, C. Zhong, Y. Zhu, X. Chen, and Z. Zhang, "Programmable metasurface based multicast systems: Design and analysis," *IEEE J. Sel. Areas Commun.*, vol. 38, no. 8, pp. 1763–1776, Aug. 2020.

[14] J. Zhang, Y. Zhang, C. Zhong, and Z. Zhang, "Robust design for intelligent reflecting surfaces assisted MISO systems," *IEEE Commun. Lett.*, vol. 24, no. 10, pp. 2353–2357, Oct. 2020.

[15] C. Huang, A. Zappone, G. C. Alexandropoulos, M. Debbah, and C. Yuen, "Reconfigurable intelligent surfaces for energy efficiency in wireless communication," *IEEE Trans. Wireless Commun.*, vol. 18, no. 8, pp. 4157–4170, Aug. 2019.

[16] Q. Wu and R. Zhang, "Towards smart and reconfigurable environment: intelligent reflecting surface aided wireless network," *IEEE Commun. Mag.*, vol. 58, no. 1, pp. 106–112, Jan. 2020.

[17] W. Yan, X. Yuan, Z. He, and X. Kuai, "Passive beamforming and information transfer design for reconfigurable intelligent surfaces aided multiuser MIMO systems," *IEEE J. Sel. Areas Commun.*, vol. 38, no. 8, pp. 1793–1808, Aug. 2020.

[18] W. Yan, X. Yuan, and X. Kuai, "Passive beamforming and information transfer via large intelligent surface," *IEEE Wireless Commun. Lett.*, vol. 9, no. 4, pp. 533–537, Apr. 2020.

[19] M. Jung, W. Saad, M. Debbah, and C. S. Hong, "On the optimality of reconfigurable intelligent surfaces (RISs): Passive beamforming, modulation, and resource allocation," *IEEE Trans. Wireless Commun.*, pp. 1–1, 2021.

[20] H. Guo, Y. Liang, J. Chen, and E. G. Larsson, "Weighted sum-rate maximization for reconfigurable intelligent surface aided wireless networks," *IEEE Trans. Wireless Commun.*, vol. 19, no. 5, pp. 3064–3076, May 2020.

[21] K. Ying, Z. Gao, S. Lyu, Y. Wu, H. Wang, and M. Alouini, "GMD-based hybrid beamforming for large reconfigurable intelligent surface assisted millimeter-wave massive MIMO," *IEEE Access.*, vol. 8, pp. 19530–19539, Jan. 2020.

[22] Q. Wu and R. Zhang, "Intelligent reflecting surface enhanced wireless network via joint active and passive beamforming," *IEEE Trans. Wireless Commun.*, vol. 18, no. 11, pp. 5394–5409, Nov. 2019.

[23] Q. Wu and R. Zhang, "Beamforming optimization for wireless network aided by intelligent reflecting surface with discrete phase shifts," *IEEE Trans. Commun.*, vol. 68, no. 3, pp. 1838–1851, Mar. 2020.

[24] T. L. Jensen and E. De Carvalho, "An optimal channel estimation scheme for intelligent reflecting surfaces based on a minimum variance unbiased estimator," in *Proc. IEEE International Conference on Acoustics, Speech and Signal Processing (ICASSP)*, 2020, pp. 5000–5004.

[25] Q. -U. -A. Nadeem, H. Alwazani, A. Kammoun, A. Chaaban, M. Debbah, and M. -S. Alouini, "Intelligent reflecting surface-assisted multi-user MISO communication: Channel estimation and beamforming design," *IEEE Open J. Commun. Soc.*, vol. 1, pp. 661–680, 2020.

[26] X. Guan, Q. Wu, and R. Zhang, "Anchor-assisted intelligent reflecting surface channel estimation for multiuser communications," arXiv:2008.00622v1, 2020. [Online]. Available: https://arxiv.org/abs/2008.00622v1.

[27] L. Wei, C. Huang, G. C. Alexandropoulos, C. Yuen, Z. Zhang, and M. Debbah, "Channel estimation for RIS-empowered multi-user MISO wireless communications," *IEEE Trans. Commun.*, pp. 1–1, 2021.

[28] M. Jung, W. Saad, and G. Kong, "Performance analysis of active large intelligent surfaces (LISs): Uplink spectral efficiency and pilot training," *IEEE Trans. Commun.*, vol. 69, no. 5, pp. 3379–3394, May 2021.

[29] G. C. Alexandropoulos and E. Vlachos, "A hardware architecture for reconfigurable intelligent surfaces with minimal active elements for explicit channel estimation," in *Proc. IEEE International Conference on Acoustics, Speech and Signal Processing (ICASSP),* May. 2020. pp. 9175–9179.

[30] C. Chaccour, M. N. Soorki, W. Saad, M. Bennis, and P. Popovski, "Risk-based optimization of virtual reality over Terahertz reconfigurable intelligent surfaces," in *Proc. 2020 IEEE International Conference on Communications (ICC)*, Jun. 2020. pp. 1–6.

[31] C. Huang, G. C. Alexandropoulos, C. Yuen, and M. Debbah, "Indoor signal focusing with deep learning designed reconfigurable intelligent surfaces," in *Proc. 2019 IEEE 20th International Workshop on Signal Processing Advances in Wireless Communications (SPAWC)*, Jul. 2019. pp. 1–5.

[32] X. Liu, Y. Liu, Y. Chen, and H. V. Poor, "RIS enhanced massive non-orthogonal multiple access networks: deployment and passive beamforming design," *IEEE J. Sel. Areas Commun.*, vol. 39, no. 4, pp. 1057–1071, Apr. 2021.

[33] H. Huang, J. Yang, H. Huang, Y. Song, and G. Gui, "Deep learning for super-resolution channel estimation and DOA estimation based massive MIMO system," *IEEE Trans. Veh. Technol.*, vol. 67, no. 9, pp. 8549–8560, Sept. 2018.

[34] H. He, C. Wen, S. Jin, and G. Y. Li, "Deep learning-based channel estimation for beamspace mmWave massive MIMO systems," *IEEE Wireless Commun. Lett.*, vol. 7, no. 5, pp. 852–855, Oct. 2018.

[35] Y. Han, M. Li, S. Jin, C. Wen, and X. Ma, "Deep learning based FDD non-stationary massive MIMO downlink channel reconstruction," *IEEE J. Sel. Areas Commun.*, vol. 38, no. 9, pp. 1980–1993, Sept. 2020.

[36] H. Wang, X. Li, and T. Zhang, "Generative adversarial network based novelty detection using minimized reconstruction error," *Frontiers of Information Technology & Electronic Engineering*, vol. 19, no. 1, pp. 116–125, 2018.

[37] C. Xing, S. Wang, S. Chen, S. Ma, H. V. Poor, and L. Hanzo, "Matrix-monotonic optimization - part I: Single-variable optimization," *IEEE Trans. Signal Process.*, vol. 69, pp. 738–754, 2021.

[38] X. Ma and Z. Gao, "Data-driven deep learning to design pilot and channel estimator for massive MIMO," *IEEE Trans. Veh. Technol.*, vol. 69, no. 5, pp. 5677–5682, May 2020.

[39] Y. Yang, S. Zhang, F. Gao, J. Ma, and O. A. Dobre, "Graph neural network based channel tracking for massive MIMO networks," *IEEE Commun. Lett.*, vol. 24, no. 8, pp. 1747–1751, Aug. 2020.

[40] Y. Yang, F. Gao, X. Ma, and S. Zhang, "Deep learning-based channel estimation for doubly selective fading channels," *IEEE Access.*, vol. 7, pp. 36579–36589, Apr. 2019.

[41] S. Khan and S Y. Shin, "Deep-learning-aided detection for reconfigurable intelligent surfaces," arXiv:1910.09136v1, 2019. [Online]. Available: https://arxiv.org/abs/1910.09136v1.

[42] J. Gao, C. Zhong, X. Chen, H. Lin, and Z. Zhang, "Unsupervised learning for passive beamforming," *IEEE Commun. Lett.*, vol. 24, no. 5, pp. 1052–1056, May 2020.

[43] C. Huang, R. Mo, and C. Yuen, "Reconfigurable intelligent surface assisted multiuser MISO systems exploiting deep reinforcement learning," *IEEE J. Sel. Areas Commun.*, vol. 38, no. 8, pp. 1839–1850, Aug. 2020.

[44] M. Alrabeiah and A. Alkhateeb, "Deep learning for TDD and FDD massive MIMO: Mapping channels in space and frequency," in *Proc. Asilomar Conference on Signals, Systems, and Computers*, Nov. 2019. pp. 1465–1470.

[45] A. Taha, M. Alrabeiah, and A. Alkhateeb, "Enabling large intelligent surfaces with compressive sensing and deep learning," *IEEE Access.*, vol. 9, pp. 44304–44321, 2021.

[46] P. Dong, H. Zhang, and G. Y. Li, "Machine learning prediction based CSI acquisition for FDD massive MIMO downlink," in *Proc. IEEE Global Communications Conference (GLOBECOM)*, Dec. 2018, pp. 1–6

[47] Y. Liu, S. Zhang, F. Gao, J. Ma, and X. Wang, "Uplink-aided high mobility downlink channel estimation over massive MIMO-OTFS system," *IEEE J. Sel. Areas Commun.*, vol. 38, no. 9, pp. 1994–2009, Sept. 2020.

[48] A. Alkhateeb, "DeepMIMO: A generic deep learning dataset for millimeter wave and massive MIMO applications," in *Proc. Information Theory and Applications Workshop (ITA)*, (San Diego, CA), Feb. 2019, pp. 1–8,.

[49] I. A. Huijben, B. S. Veeling, and R. J. van Sloun, "Deep probabilistic subsampling for task-adaptive compressed sensing," in *International Conference on Learning Representations*, 2019.

[50] E. J. Gumbel, "Statistical theory of extreme values and some practical applications," *NBS Applied Mathematics Series*, vol. 33, 1954.

[51] D. P. Kingma and J. Ba, "ADAM: A method for stochastic optimization," arXiv:1412.6980v9, 2019. [Online]. Available: https://arxiv.org/abs/arXiv:1412.6980v9.

[52] G. E. Hinton, N. Srivastava, A. Krizhevsky, I. Sutskever, and R. R. Salakhutdinov, "Improving neural networks by preventing co-adaptation of feature detectors," arXiv:1207.0580v1, 2012. [Online]. Available: https://arxiv.org/abs/arXiv:1207.0580v1.

[53] Remcom, "Wireless insite," http://www.remcom.com/wireless-insite.

[54] Y. Yang, F. Gao, G. Y. Li, and M. Jian, "Deep learning-based downlink channel prediction for FDD massive MIMO system," *IEEE Commun. Lett.*, vol. 23, no. 11, pp. 1994–1998, Nov. 2019.

Shunbo Zhang received the B.S. degree in communication engineering from Xidian University, Xi'an, China, in 2019. He is currently working toward the M.S. degree with the State Key Laboratory of Integrated Services Networks, Xidian University, Xi'an, China.

His research interests include MIMO-OFDM systems, RIS assisted communications, and deep learning for communication systems.

Shun Zhang (Senior Member, IEEE) received the B.S. degree in communication engineering from Shandong University, Jinan, China, in 2007, and the Ph.D. degree in communications and signal processing from Xidian University, Xian, China, in 2013.

He is currently with the State Key Laboratory of Integrated Services Networks, Xidian University, where he is currently an Associate Professor. His research interests include massive MIMO, millimeter wave systems, RIS assisted communications, deep learning for communication systems, orthogonal time frequency space (OTFS) systems, and multiple access techiques. He is an Editor for Physical Communication. He has authored or coauthored more than 80 journal and conference papers, and is the inventor of 16 granted patents (including a PCT patent authorized by US Patent and Trademark Office). He has received two Best Paper Awards in conferences, and two prize awards in natural sciences for research excellence by both China Institute of Communications and Chinese Institute of Electronics.

Feifei Gao (Fellow, IEEE) received the B.Eng. degree from Xi'an Jiaotong University, Xi'an, China in 2002, the M.Sc. degree from McMaster University, Hamilton, ON, Canada in 2004, and the Ph.D. degree from National University of Singapore, Singapore in 2007. Since 2011, he joined the Department of Automation, Tsinghua University, Beijing, China, where he is currently an Associate Professor.

Prof. Gao's research areas include communication theory, signal processing for communications, artificial Intelligence for communications, array signal processing, and convex optimizations. He has authored/coauthored more than 120 refereed IEEE journal papers and more than 120 IEEE conference proceeding papers.

Prof. Gao has served as an Editor of IEEE Transactions on Wireless Communications, IEEE Transactions on Cognitive Communications and Networking, IEEE Signal Processing Letters, IEEE Communications Letters, IEEE Wireless Communications Letters, and China Communications. He has also served as the symposium co-chair for 2019 IEEE Conference on Communications (ICC), 2018 IEEE Vehicular Technology Conference Spring (VTC), 2015 IEEE Conference on Communications (ICC), 2014 IEEE Global Communications Conference (GLOBECOM), 2014 IEEE Vehicular Technology Conference Fall (VTC), as well as Technical Committee Members for many other IEEE.

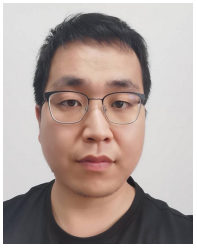

Jianpeng Ma (Member, IEEE) was born in Gansu, China, in 1990. He received the B.S. and Ph.D. degrees from Xidian University, Xi'an, China, in 2012 and 2018, respectively. From 2016 to 2018, he was a visiting student with the Department of Electrical and Computer Engineering, McMaster University, Hamilton, ON, Canada.

He is currently with the State Key Laboratory of Integrated Services Networks, Xidian University. His research interests include multiple-inputmultiple-output (MIMO) techniques, massive MIMO systems, cooperative communication, and satellite communication.

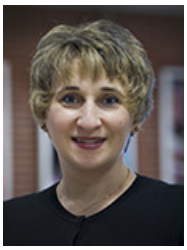

Octavia A. Dobre (Fellow, IEEE) received the Dipl. Ing. and Ph.D. degrees from the Polytechnic Institute of Bucharest, Romania, in 1991 and 2000, respectively. Between 2002 and 2005, she was with New Jersey Institute of Technology, USA. In 2005, she joined Memorial University, Canada, where she is currently Professor and Research Chair. She was a Visiting Professor with Massachusetts Institute of Technology, USA and Université de Bretagne Occidentale, France.

Her research interests encompass enabling technologies for B5G including intelligence reflective surfaces, as well as blind signal identification, and optical and underwater communications. She co-authored over 300 refereed journal papers in these areas.

Dr. Dobre serves as the Editor-in-Chief (EiC) of the IEEE Open Journal of the Communications Society, as well as Editor of the IEEE Communications Surveys and Tutorials and IEEE Vehicular Technology Magazine. She was the EiC of the IEEE Communications Letters, Senior Editor, Editor, and Guest Editor for various prestigious journals and magazines. Dr. Dobre was the General Chair, Technical Program Co-Chair, Tutorial Co-Chair, and Technical Co-Chair of symposia at numerous conferences.

Dr. Dobre was a Royal Society Scholar and a Fulbright Scholar. She obtained Best Paper Awards at various conferences, including IEEE ICC, IEEE Globecom, and IEEE WCNC. Dr. Dobre is a Distinguished Lecturer of the IEEE Communications Society and a Fellow of the Engineering Institute of Canada.